SAFETY IN MINES RESEARCH ADVISORY COMMITTEE

FINAL REPORT

Bagged Stone Dust Barrier Evaluations in a Bord and Pillar mine

J J L du Plessis[1], E S Weiss[2] and K L Cashdollar[2]

Research Agency: 1. CSIR Miningtek, Pretoria, South Africa
2. National Institute for Occupational Safety and Health (NIOSH), Pittsburgh Research Laboratory (PRL), Pittsburgh, Pennsylvania, U.S.A.

Project No. : COL 501 (ESH 00-0014)

Date : May 2000

Acknowledgements

This research was conducted under Memorandum of Agreement 99-PRL-03 between the U.S. National Institute for Occupational Safety and Health and the Council of Scientific and Industrial Research of South Africa.

The authors wish to thank the following project team members for their assistance in the preparation and the execution of the test program at the Lake Lynn Laboratory (LLL). All are from the PRL.

Deepak Kohli	Electrical Engineer
Kenneth Jackson	Electronics Technician
William Slivensky	Physical Science Technician
Donald Sellers	Physical Science Technician
Frank Karnack	Physical Science Technician
Gregory Green	Physical Science Technician

The following PRL personnel assisted in preparing the instrumentation for the tests.

Michael Sapko	Senior Research Physical Scientist
Richard Thomas	Electronics Technician

The following PRL personnel prepared the dust mixtures for the tests.

Paul Stefko	Miner Mechanic
Samuel Angelo	Miner Mechanic
Jack Teatino	Miner Mechanic

Executive Summary

The project was successfully completed at the National Institute for Occupational Safety and Health (NIOSH), Pittsburgh Research Laboratory's (PRL), Lake Lynn Experimental Mine (LLEM) during the period from January 1999 through May 2000. The tests were conducted in a three-entry section of LLEM.

The prime objective of Phase I (January 1999 through April 1999) of the work was to evaluate single bag performance at various positions in the gallery when exposed to different explosions. These methane explosions varied in strength and position to generate varied explosion pulses and explosion generation directions.

The evaluation of the functional performance of the bags included visual inspections of the bags and an estimation of the stone dust distribution on the mine floor after the explosions.

The major conclusions of the work can be summarised as follows:

- That a bag can operate at dynamic pressure as low as 4 kPa.
- The static pressure is reduced and almost reaches equilibrium in the three entries at distances far (>100 m) from the ignition position in B-drift.
- Stone dust bags suspended in these areas of pressure equalization (in the crosscuts between the entries) did not operate effectively.

It can be concluded that the pressure pulse created in a single methane explosion can result in effective bag operation in a low seam (~2 m high), multiple entry mine when suspended close to the roof. The effective distribution of stone dust is dependent on the distance from the explosion source as well as the position or placement of the bag, i.e., if it is suspended in a drift or a crosscut. It was further noted that the total dust dispersal efficiency is less for multiple entry tests when compared to previous test work in single entry tests.

The prime objective of the tests against coal dust explosions (Phase II of the project conducted from October 1999 through March 2000) was to evaluate the distributed and concentrated bagged barrier performance in a multi-entry mine section. To this end two evaluation explosions were used. The fuel zone of the first explosion type was only in the

center B-drift, and the barrier was also installed in B-drift. The distributed barrier extended from about 74 to 170 m and the concentrated barrier extended from about 74 to 104 m in B-drift. In the second explosion type, coal-rock dust fuel mixtures were placed in all three drifts. A total of six explosions, two baseline and four barrier evaluation explosions, were conducted. Two explosions each were used to evaluate the distributed and concentrated barriers

The distributed barrier was successful in both types of explosion tests in inhibiting flame propagation. The flame extended further for the explosion tests where the dust was loaded in all three entries compared with dust loaded only in the center entry, but in both cases the flame was stopped within the barrier zone. The concentrated barrier was also successful in stopping flame propagation within the barrier zone in both explosion tests.

From the full-scale experimental mine test results, it can be concluded that both bagged barrier designs were effective in stopping coal dust explosions in the multiple entries of the LLEM.

Table of contents

Appendices

List of Figures

List of Tables

Glossary of abbreviations, symbols and terms

Abbreviations

LLEM	Lake Lynn Experimental Mine
PRL	Pittsburgh Research Laboratory
NIOSH	National Institute for Occupational Safety and Health
TIC	Total Incombustible Content
LTR	Last Through Road
IR	Infrared
PPC	Pittsburgh pulverized coal
USBM	United States Bureau of Mines
Eff.	Efficiency

Symbols

g/m^3	grams per cubic meter
J	joule
kg	kilogram
km	kilometer
km^2	square kilometer
kPa	kilopascal
m	metre
m^2	square metre
m^3	cubic metre
ms	millisecond
m/s	meters per second
psi	pound (force) per square inch, gauge
psia	pound (force) per square inch, absolute
s	second
t	ton (metric)
V	volt
%	percent

1 Introduction

During the past three decades, the South African coal mining industry has experienced a significant number of explosions leading to a considerable loss of life. Since 1993 the strategic thrust of local research has been to prevent the accumulation of methane by good ventilation practice, a to eliminate frictional sparking by the use of water sprays, to minimize dust generation and dispersion, and to use stone dust to prevent coal dust explosion.

The final line of defense, however, is the use of barriers to prevent a coal dust explosion from propagating. Over the past four or five years, a great deal of research has been conducted on developing a bagged stone dust barrier.

Following the successful selection of bag material and the development of closure mechanisms, the bags have proved effective in suppressing explosions in the gallery at Kloppersbos (5 m^2 cross sectional area) and at the experimental mine at Tremonia, Germany (20 and 22 m^2 cross sectional areas). This demonstrated that the concept of a bagged stone dust barrier could be used with considerable confidence in protecting long single entries.

However, in South African coal mines, multiple entry mining methods are invariably used but little was known of how explosions propagate under these conditions. As it is known that crosscuts can cause attenuation of the pressure waves associated with explosions and that the simultaneous arrival of pressure waves from different directions may well render the bag breakage mechanism ineffective, it was important that the final series of tests for these barriers be conducted in a room and pillar section. In particular, it was essential to determine whether or not bagged stone dust barriers can effectively suppress coal dust explosions in room and pillar sections. The National Institute for Occupational Safety and Health (NIOSH), Pittsburgh Research Laboratory's (PRL), Lake Lynn Experimental Mine (LLEM) is the only facility worldwide where suitable tests could be conducted in a room and pillar section.

2 Lake Lynn Experimental Mine

2.1 Description of LLEM

The Lake Lynn Laboratory (LLL) is located approximately 80 km southeast of Pittsburgh, near Fairchance, Pennsylvania, U.S.A. The facility occupies more than 1,6 km^2 at a former commercial limestone mine. This site was formerly developed in the 1950's as a limestone quarry, with underground room and pillar workings excavated from the highwall. Due to changes in mining geometries and the need for isolation for conducting large-scale explosion research, the U. S. Bureau of Mines (USBM) developed the LLL in the early 1980's. Even though the principal purpose for constructing the laboratory was mine explosion testing, the underground experimental mine design, expansive surface areas, and modern data-gathering and computer systems afforded an opportunity for a broad range of mine safety and health research. In October 1996, the PRL facility, including the LLL, was transferred from the USBM to NIOSH.

Mattes, Bacho and Wade (1983) described the development of the site. The underground workings consist of two distinct sections:

- There are approximately 7620 m of 16 m wide by 9 m high entries that were developed in the mid 1960's as part of the commercial limestone mining operation. In recent years, portions of this section near the highwall have proved to be unstable, with roof collapses causing subsidence through to the top of the mountain. This has resulted in two of the four portals being closed and this area of the mine being abandoned.
- The 2286 m of new workings were developed by the USBM. The dimensions of the drifts and crosscuts are typical of modern U.S. geometries for coal mine entries and range from 5,5 to 6,0 m wide and approximately 2 m high. The average cross sectional area of the entries is 11,5 m^2. The LLEM was designed to withstand explosion overpressures up to approximately 700 kPa (100 psi). The layout of both the old and the new workings is shown in Figure 2.1.

Two movable, explosion-resistant bulkheads allow the LLEM to simulate 5 discrete mining layouts:

1) an entire mine
2) a single entry
3) a triple entry
4) a longwall face with a single entry
5) a longwall face with a triple entry

In order to simulate room and pillar workings, drifts A, B, and C are isolated from E drift by closing the bulkhead at that point. The three drifts are approximately 520 m long, with seven crosscuts at the inbye end. The pillars created by this configuration are each approximately 24 m long by 11 m wide.

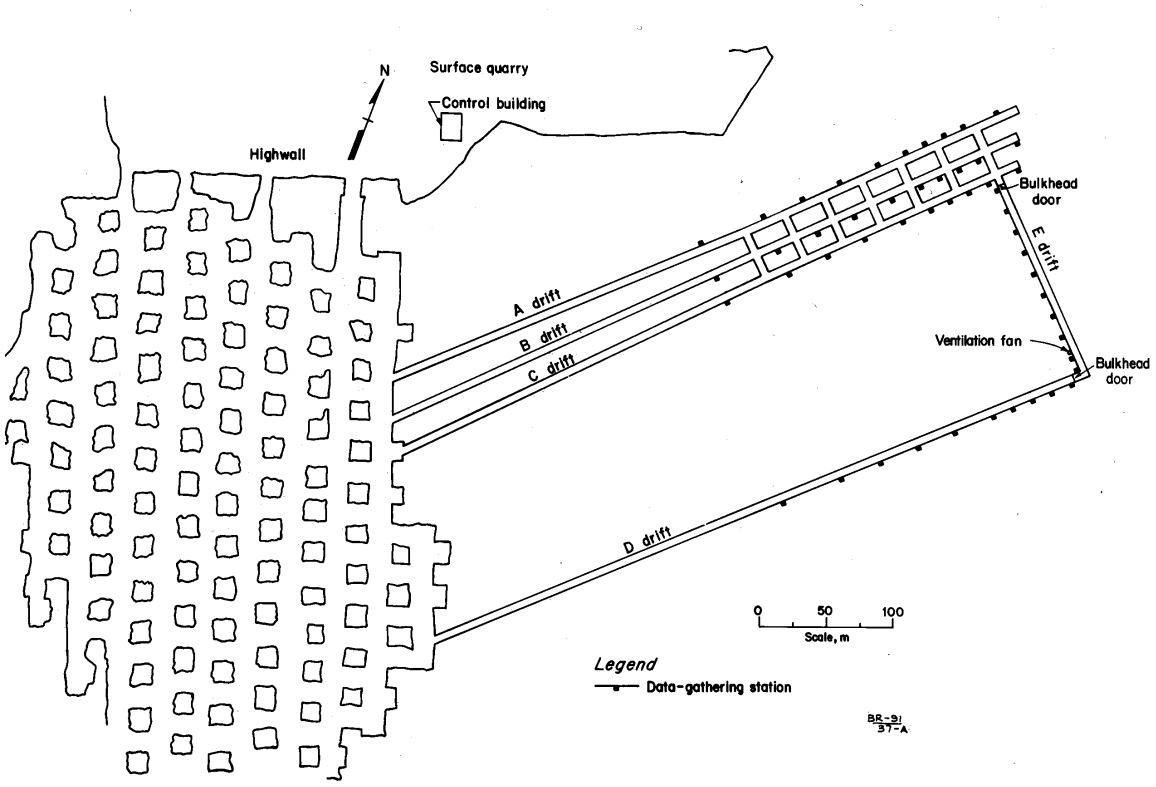

Figure 2.1 General plan of Lake Lynn experimental mine

3 Equipment and instrumentation

3.1 Static pressure and flame measurements

Each LLEM drift has ten environmentally controlled data-gathering (DG) stations (locations shown in Figure 2.1) inset in the rib wall. Each data-gathering station houses a strain gauge transducer to measure the explosion pressure and an optical sensor to detect the flame arrival. The pressure transducer is perpendicular to the entry length and therefore measures the static pressure generated by the explosion. The pressure transducers were from Dynisco, Viatran, or Genisco. They were rated at 0-690 kPa (0-100 psia), with 0-5 V output, infinite resolution, and response time less than 1 ms. The flame sensors used Texas Instrument Type LS400 silicon phototransistors and Optek Type OP598A photosensors, both with response times on the order of microseconds. These devices were positioned back from the front window of the flame sensors in order to limit the field of view. The instrument positions for the individual instruments are summarised in Table 3.1.

Table 3.1

Optical flame sensor and static pressure transducer positions at the data gathering (DG) panels on the ribs

A-drift		**B-drift**		**C-drift**	
DG Station	**Distance from A-drift face (m)**	**DG Station**	**Distance from B-drift face (m)**	**DG Station**	**Distance from C-drift face (m)**
A-1	6,7	B-1	3,0	C-1	4,0
A-2	40,2	B-2	32,9	C-2	25,6
A-3	55,8	B-3	48,2	C-3	40,8
A-4	71,0	B-4	64,3	C-4	56,1
A-5	86,3	B-5	78,3	C-5	71,3
A-6	108,2	B-6	100,3	C-6	92,7
A-7	138,1	B-7	130,1	C-7	122,8
A-8	167,6	B-8	160,3	C-8	152,7
A-9	197,8	B-9	190,8	C-9	182,3
A-10	246,0	B-10	238,4	C-10	230,7

3.2 Dynamic pressure measurements

In the evaluation of an explosion barrier, it is also essential that the dynamic pressure approaching the barrier position be known. This is normally used to relate the barrier operation to a rated dynamic pressure. For this program, a minimum of three dynamic pressure measurements were obtained; one in each of A, B, and C drifts. Two types of dynamic pressure sensors were used: the Kistler dynamic pressure sensor (Kistler 9203, similar to those used at DMT and Kloppersbos) and the PRL differential pressure probe, using the principle of:

$$VP = TP - SP$$

where: VP = dynamic pressure
TP = total pressure
SP = static pressure

A total of 6 PRL probes and 3 Kistler transducers were installed on various platforms/stands in the middle of the entries or crosscuts. The positions of the instrument platforms/stands are listed in Table 3.2. The position of each stand is identified in the table by the drift letter and the distance from the face in meters. The crosscut position (listed as X-2) was the second crosscut between B- and C-drifts. The actual positions of the dynamic pressure instruments were altered as the ignition position was altered. The positions of the two sensor types for the individual tests are listed in the relevant tables in the results sections of the report.

Also included on some instrument stands was a simplistic device to measure the static explosion pressure. This device utilized a standard tire pressure gauge positioned perpendicular to the explosion pressure pulse. Preliminary results have shown that this tire gauge device can provide a reasonably close approximation of the static pressure generated during the explosion. This device was designed to provide an inexpensive, yet reliable, method for measuring low-level explosions that may occur within remote sealed areas of a mine.

Table 3.2

Dynamic pressure instrument positions

A-Drift	B-Drift	Crosscut	C-Drift
Platform or Stand Position (m)	**Platform or Stand Position (m)**	**Platform or Stand Position**	**Platform or Stand Position (m)**
A-49	B-41		C-34
A-79	B-73	X-2	C-64
	B-101		
	B-130		

Figure 3.2 is a photograph of one of the instrument stands showing the positions of the Kistler dynamic pressure sensor (the small disk on the end of the rod extending in front of the mining engineer) and the PRL differential pressure probe (the tubing extending to the left of the platform). Also seen on the right in the photo are several bags of rock dust that will be installed in the barrier.

Figure 3.2: Instrument stand with the two different dynamic pressure instruments

3.3 Temperature measurements

Since the measurement of explosion temperature at the barrier positions proved valuable in barrier evaluations done at the DMT Tremonia Experimental Mine (Michelis, Margenburg and du Plessis, 1996 and Margenburg and du Plessis, 1996 final), NIOSH was requested to measure temperatures at each individual barrier position. The total heat flux from the LLEM explosions was measured using Thermogage sensors that operated on the Gardon principle (Gardon, 1953). These heat flux gauges were installed at the following positions: B-64 and B-100.

The temperature was calculated from the total heat flux using the Stefan-Boltzmann Law:

$$H = \Phi T^4 ,$$

where:

H is heat flux (W cm^{-2})

Φ is a constant (5,67 x 10^{-12} W cm^{-2} K^{-4})

T is temperature in Kelvin (K)

3.4 Data capturing system

The sensor data gathered during the explosion tests were relayed from each of the data-gathering stations to an underground instrument room off C-drift and then to an outside control building. A high-speed, 64-channel, PC-based computer data acquisition system (DAS) was used to collect and analyze the data. This system collected the sensor data at a rate of 1500 samples/s over a 5-s period. The data were then processed using LabView, Excel, and PSI-Plot software and outputted in graphic and tabular form as will be shown and discussed in the "Test Results" section and Appendices. The reported pressure data were averaged over 10 ms (15 point smoothing). As a back-up, the data were also collected on an older microVAX computer system.

3.5 Gas ignition zone

Before each explosion test, a 60-t hydraulically operated, track-mounted, concrete and steel bulkhead door was positioned across E-drift to confine the explosion pressures to the A,B,C-

drift multiple entry area. Natural gas (~97% methane) was remotely injected into the face area (closed end) of either B- or C-drift. An electric fan with an explosion-proof motor housing was used to mix the natural gas with air in the ignition zone.

A plastic diaphragm was used to contain the natural gas and air mixture within the closed end of the drift; the size of the ignition zone varied depending on the desired pressure levels for a particular test. A gas sampling tube within the ignition zone was used to continuously pull a sample and monitor the gas concentration using an infrared analyzer. In addition, samples were collected in evacuated test tubes and sent to the PRL analytical laboratory for more accurate analyses using a gas chromatograph. These analyses were used to verify the infrared analyzer readings.

Electrically activated 100 J matches, generally in a triple-point configuration across the face (closed end) of the entry, were used to ignite the flammable natural gas and air mixtures. For some of the tests, barrels filled with water were located in the gas ignition zone to act as turbulence generators to achieve a higher projected pressure pulse.

4 Selected past experiments at LLEM

One of the original objectives of establishing LLEM was to study the effect of multiple entries on the strength and propagation of methane and coal dust explosions, but only limited work in this area had been completed before this project. Greninger, Cortese and Weiss, 1995, have described some of this work. A summary of some of the baseline test configurations conducted during this program is shown in Table 4a.

Table 4a

Summary of previous baseline test configurations

Test	Drift	Ignition zone	Coal dust loading
#268	B	12,2 m – gas	None
#269	B	21,3 m – gas	None
#270	B	12,2 m – gas	100 g/m^3 at B15 – 40 m
#271	B	12,2 m – gas	100 g/m^3 at B15 – 40 m & in 1st x-cuts
#292	D	12,2 m – gas	None
#293	D	12,2 m – gas	100 g/m^3 at D12 – 40 m
#296	D	12,2 m – gas	50 g/m^3 at D15 – 40 m
#317	C	14,3 m – gas	100 g/m^3 at C15 – 40 m
#318	C	12,2 m – 200 g/m^3	None
#319	C	12,2 m – 200 g/m^3	100 g/m^3 at C15 – 40 m
#320	C	14,3 m – gas	None
#321	B	12,2 m – gas	200 g/m^3 at B15 – 40 m & in 1st x-cuts
#323	C	14,3 m – gas	100 g/m^3 at C13 – 78 m & seals

5 Program of Work

The overriding objectives of this project were to ensure that the program would:

a) show whether stone dust bags would rupture and distribute the stone dust during a room-and-pillar explosion; and

b) show whether coal dust explosions in room-and-pillar workings can be suppressed by bagged stone dust barriers.

Since methane explosions are relatively inexpensive and can be performed quickly, all of Phase I of the proposed work was undertaken using methane explosions. Coal dust

explosions in multiple entries take several days to set up and up to three weeks to clean up afterwards and so only a limited number of these tests could be conducted.

5.1 Description of methane tests (Phase I)

The program of work called for a minimum of 18 methane-air explosions to be conducted, with six being baseline experiments to determine the static and dynamic pressures throughout the multiple entry zone of LLEM. By varying the ignition source, volume, and composition of the methane zone; strong, medium and weak explosions were generated. Replications of individual tests were undertaken to determine the reproducibility of the results. For most of the gas explosion tests, a substantial seal was located in crosscut 1 between B- and C-drifts. For the last four explosion tests, this seal was removed.

After the baseline tests were completed, further tests were conducted with single bags suspended from the mine roof at various locations throughout the multiple entry zone. The specific positions of the stone dust bags are shown in Figure 5.1.a.

Figure 5.1a: Bag positions

The objective of these tests was to determine the bags' rupture characteristics as well as the distribution pattern of the stone dust under varying pressure regimes. Some bags were suspended in the intersections (Figure 5.1.b), others in the crosscuts (splits) throughout A, B, and C drifts (Figure 5.1c).

Figure 5.1b: Stone dust bag suspended in the mine entry

Figure 5.1c: Installation of individual stone dust bag in crosscut

In Table 5.1a, a short description of the baseline gas tests (LLEM tests #367 to #372) is given. The first column lists the LLEM test number, the second column lists the date of the test, and the last column provides a short description of the test.

Table 5.1a

Methane baseline test descriptions

Test	Date	Explosion description
#367	13 Jan 99	The ignition zone was made up of a 9,5% gas/air volume concentration, which extended up to 14,3 m in C-drift (approximately 171,6 m^3 gas/air mixture). The gas mixture was ignited at the face using triple point ignition. The electric matches were equally space across the closed end of the face. Water-filled barrels were used across the gas zone to act as turbulence generators.
368	22 Jan 99	The ignition zone was made up of a 9,5% gas/air volume concentration, which extended up to 14,3 m in C-drift (approximately 171,6 m^3 gas/air mixture). The gas mixture was ignited at the face using triple point ignition. The electric matches were equally space across the closed end of the face. Water-filled barrels were used across the gas zone to act as turbulence generators.
#369	27 Jan 99	The ignition zone was made up of an 8,5% gas/air volume concentration, which extended up to 8,2 m in C-drift (approximately 99,6 m^3 gas/air mixture). The gas mixture was ignited at the face using a single ignition. No water-filled barrels were used.
#370	1 Feb 99	The ignition zone was made up of a 9,5% gas/air volume concentration, which extended up to 14,3 m in C-drift (approximately 171,6 m^3 gas/air mixture). The gas mixture was ignited at the face using triple point ignition. The electric matches were equally space across the closed end of the face. No water-filled barrels were used.
#371	5 Feb 99	The ignition zone was made up of a 9,5% gas/air volume concentration, which extended up to 12,2 m in B-drift (approximately 146,4 m^3 gas/air mixture). The gas mixture was ignited at the face using triple point ignition. The electric matches were equally space across the closed end of the face. No water-filled barrels were used.
#372	10 Feb 99	The ignition zone was made up of a 9,0% gas/air volume concentration, which extended up to 12,2 m in C-drift (approximately 146,6 m^3 gas/air mixture). The gas mixture was ignited at the face using triple point ignition. The electric matches were equally space across the closed end of the face. Water-filled barrels were used across the gas zone to act as turbulence generators.

Table 5.1b provides a description of the tests conducted against the individually suspended bags using the B-drift ignition zone with the seal installed in crosscut 1.

Table 5.1b

B-drift ignitions with the seal in crosscut 1

Test Nr.	Date	Explosion description
#373	16 Feb 99	The ignition zone was made up of a 9,5 per cent gas/air volume concentration, which extended up to 12,2 m in B-drift (approximately 146,4 m^3 gas/air mixture). The gas mixture was ignited at the face using triple point ignition. The electric matches were equally space across the closed end of the face. Water-filled barrels were used across the gas zone to act as turbulence generators.
#374	18 Feb 99	The ignition zone was made up of a 9,5 per cent gas/air volume concentration, which extended up to 12,2 m in B-drift (approximately 146,4 m^3 gas/air mixture). The gas mixture was ignited at the face using triple point ignition. The electric matches were equally space across the closed end of the face. Water-filled barrels were used across the gas zone to act as turbulence generators.
#375	22 Feb 99	The ignition zone was made up of an 9,5% gas/air volume concentration, which extended up to 12,2 m in B-drift (approximately 146,4 m^3 gas/air mixture). The gas mixture was ignited at the face using a triple point ignition. No water-filled barrels were used.
#376	25 Feb 99	The ignition zone was made up of a 9,5% gas/air volume concentration, which extended up to 21,3 m in B-drift (approximately 256 m^3 gas/air mixture). The gas mixture was ignited at the face using triple point ignition. The electric matches were equally space across the closed end of the face. Water filled barrels was used across the gas zone to act as turbulence generators.
#377	2 March 99	The ignition zone was made up of a 9,5% gas/air volume concentration, which extended up to 21,3 m in B-drift (approximately 256 m^3 gas/air mixture). The gas mixture was ignited at the face using triple point ignition. The electric matches were equally space across the closed end of the face. No water-filled barrels were used.
#378	4 March 99	The ignition zone was made up of a 9,5% gas/air volume concentration, which extended up to 12,2 m in B-drift (approximately 146,4 m^3 gas/air mixture). The gas mixture was ignited at the face using triple point ignition. The electric matches were equally space across the closed end of the face. No water-filled barrels were used.

Table 5.1c lists the description of each test conducted against the individually suspended barrier bags using the B-drift ignition zone without the seal in crosscut 1.

Table 5.1c

B-drift ignitions without the seal

Test Nr.	Date	Explosion description
#383	31 March 99	The ignition zone was made up of a 9,5% gas/air volume concentration, which extended up to 12,2 m in B-drift (approximately 146,4 m^3 gas/air mixture). The gas mixture was ignited at the face using triple point ignition. The electric matches were equally space across the closed end of the face. Water-filled barrels were used across the gas zone to act as turbulence generators.
#384	2 Apr 99	The ignition zone was made up of a 9,5% gas/air volume concentration, which extended up to 21,3 m in B-drift (approximately 256 m^3 gas/air mixture). The gas mixture was ignited at the face using triple point ignition. The electric matches were equally space across the closed end of the face. Water filled barrels was used across the gas zone to act as turbulence generators.

Table 5.1d lists the description of each test conducted against the individually suspended barrier bags when using the C-drift ignition zone with a seal installed in crosscut 1.

Table 5.1d

C-drift ignitions with the seal

Test Nr.	Date	Explosion description
#379	8 March 99	The ignition zone was made up of a 9,5% gas/air volume concentration, which extended up to 14,3 m in C-drift (approximately 171,6 m^3 gas/air mixture). The gas mixture was ignited at the face using triple point ignition. The electric matches were equally space across the closed end of the face. No water-filled barrels were used.
#380	10 March 99	The ignition zone was made up of a 9,5% gas/air volume concentration, which extended up to 14,3 m in C-drift (approximately 171,6 m^3 gas/air mixture). The gas mixture was ignited at the face using triple point ignition. The electric matches were equally space across the closed end of the face. Water-filled barrels were used across the gas zone to act as turbulence generators.

The only difference in the two explosion tests was the use of water-filled barrels as turbulence generators in test #380. Table 5.1e lists the description of each test conducted against the individually suspended barrier bags when using the C-drift ignition zone without the seal in crosscut 1.

Table 5.1e

C-drift ignitions without the seal

Test Nr.	Date	Explosion description
#381	24 March 99	The ignition zone was made up of a 9,5% gas/air volume concentration, which extended up to 14,3 m in C-drift (approximately 171,6 m^3 gas/air mixture). The gas mixture was ignited at the face using triple point ignition. The electric matches were equally space across the closed end of the face. Water-filled barrels were used across the gas zone to act as turbulence generators.
#382	26 March 99	The ignition zone was made up of a 9,5% gas/air volume concentration, which extended up to 14,3 m in C-drift (approximately 171,6 m^3 gas/air mixture). The gas mixture was ignited at the face using triple point ignition. The electric matches were equally space across the closed end of the face. No water-filled barrels were used.

These tests were identical to tests #379 and #380 except that the seal in crosscut 1 was removed to determine its influence on the overall explosion pressure profile within the multiple entry area and resultant impact on the performance of the individually suspended barrier bags. A short summary of all the methane tests from Phase I is in Appendix 1a.

5.2 Description of coal dust explosion tests (Phase II)

The second phase of the program of work involved 6 full-scale coal dust explosions conducted from October 1999 to March 2000. Each of these dust explosion tests was initiated with the 21,3 m long B-drift gas zone. This phase of the program was originally to include three baseline experiments; two being replications with the coal and stone dust (65% stone dust) loaded only in B-drift and the third with dust loaded in all three drifts (65% stone dust in B, 80% in A and C). For each of these tests, the coal and stone dust loadings would

extend 119 m from the first outby crosscut (through road). The results of these baseline experiments would then determine whether the remaining tests against the two barrier configurations would require coal and stone dust loadings in all three drifts or only in B-drift.

Two identical tests were to be conducted against each of the two barrier configurations as installed in B-drift. The barrier was installed in B-drift to simulate a South African coal mine belt entry with only a 65% stone dust concentration; the lower stone dust concentration could result from the coal dust generated from the movement of the conveyor belt. These tests were designed to evaluate the effectiveness of the two barrier configurations in preventing flame propagation.

5.2.1 First coal dust baseline explosion: LLEM test #389

The 21,3 m long ignition zone for test #389 was the same as that used for the strong methane explosions as described for test # 384. The 82,3 m coal dust zone extended from just outbye the methane zone (21,3 m) to about 104 m. Dust was also loaded halfway into crosscuts 1 to 3. The coal dust loading was 150 g/m^3, assuming uniform dispersion throughout the cross section. The coal dust was premixed with 65% stone dust (Allegheny Mineral) resulting in a 68% total incombustible content (TIC). The total amount of coal and stone dust mixture was 560 kg, of which approximately half was suspended on shelves with the other half dispersed on the entry floor. Figure 5.2.1a shows technicians dispersing the dust mixture on the mine floor. The floor was divided into a grid pattern and an equal amount of dust mixture was dispersed onto each section of the grid. Figure 5.2.1b shows the dust mixture being placed on the roof shelves.

Figure 5.2.1a: Photograph showing coal dust distribution on floor

Figure 5.2.1b: Photograph showing coal dust distribution on shelves

5.2.2 Second coal dust baseline explosion: LLEM test #390

The second coal and stone dust baseline explosion test (#390) was identical to the first baseline test (#389), except that the dust zone was extended out to 140 m, resulting in a 119 m long dusted zone. The same 21,3 m long gas ignition zone was used for this test and the remaining coal dust explosion tests. The total amount of coal and stone dust mixture was 793 kg, of which approximately half was suspended on the roof shelves and the other half on the entry floor.

5.2.3 First distributed barrier evaluation explosion: LLEM test #391

The first test (#391) against the distributed barrier configuration used the same ignition and dust zone as baseline test #390; i.e., a 21,3 m long methane zone and a 119 m long 68% TIC dusted zone in B-drift and the halfway into crosscuts 1-3. The total amount of coal and stone dust mixture was 793 kg.

The distributed barrier configuration was divided into four equal sub barriers with the first sub barrier positioned between crosscuts 2 and 3 (barrier start position at 74 m). The other three sub barriers were positioned similarly between crosscuts 3 and 4, crosscuts 4 and 5, and crosscuts 5 and 6 with the last row of the fourth sub barrier positioned 170 m from the closed end of B-drift. Twelve, stone dust bags were suspended on each of the four, 4,8 mm diameter steel cables in each sub barrier for a total of 48 bags per sub barrier. Each bag contained 6 kg of stone dust. A total of 192 bags were used for the first evaluation of the distributed barrier configuration. The total mass of stone dust suspended in the bags was 1152 kg, resulting in an average stone dust concentration of ~96 kg/m^2 of cross section or ~1,0 kg/m^3 over the length of the barrier if all the stone dust were uniformly dispersed.

The distributed barrier layout in B-drift is shown in Figures 5.2.3a and 5.2.3b. Figure 5.2.3a shows shelves loaded with the coal and stone dust mixture between the barrier bags. In Figure 5.2.3b the details of the bag suspension method is shown. This was the farthest outbye barrier set which did not have any coal dust shelves. Each of the bags is individually hung from the horizontal wire cable, which is attached to bolts extending down from the roof.

Figure 5.2.3a: Distributed barrier layout in B-drift

Figure 5.2.3b: Stone dust bags suspension method

5.2.4 Distributed barrier: LLEM test # 392

The second test to evaluate the performance of the stone dust bags in the distributed barrier configuration was identical to the first performance test (#391) with the addition of 119 long dust zones in A- and C-drifts. The coal and stone dust used in the A- and C-drift dusted zones was premixed to provide 80% stone dust or 82% TIC. The dust was loaded on the floor and on the shelves in a manner similar to that in B-drift. The dust zone in B-drift remained the same as for test #391 (65% stone dust or 68% TIC). The triple-entry dust zones required a total of 767 kg of coal dust and 2475 kg of stone dust for a combined dust mixture of ~3242 kg.

The stone dust barrier located in B-drift was identical to that used in the previous test (#391). The first barrier started between crosscuts 2 and 3 (~74 m) and extended out to between crosscuts 5 and 6 (~170 m). In the final barrier configuration, 12 bags were suspended and equally spaced (~43 cm separation between bags) along each steel cable (fig. 5.2.3b). A total of 48 bags per sub barrier resulted in a total of 192 bags for the entire barrier. The total mass of stone dust suspended in the bags was 1152 kg, resulting in an average stone dust concentration of ~1,0 kg/m^3 over the length of the entire barrier.

5.2.5 Concentrated barrier: LLEM test # 393

The methane initiation zone and the dusted zone used for the first test to evaluate the performance of the concentrated barrier configuration was the same as that used for the first test (#391) against the distributed barrier configuration. The 119 m long dusted zone in B-drift had a coal dust concentration of 150 g/m^3 and was premixed with 65% stone dust (68% TIC).

The first row of suspended stone dust bags of this concentrated barrier system started at ~74 m (between crosscuts 2 and 3) from the closed end of B-drift. This was the same starting position as that for the distributed barrier. The other 15 rows of steel cables were equally spaced (~2 m apart) outby this position. The last row of the concentrated barrier was positioned ~104 m from the closed end (between crosscuts 3 and 4), which resulted in a nearly 30 m long concentrated barrier system. The installation of the concentrated barrier in B-drift is shown in Figures 5.2.5a and 5.2.5b. The first figure is looking inbye in B-drift from

intersection 3. The second figure is a side view of the barrier as viewed from the crosscut. A total of 12 bags was suspended and equally spaced (~43 cm separation between bags) along each of the 16 steel cables. A total of 192 bags was installed for the concentrated barrier configuration. The total mass of stone dust suspended in the bags was 1152 kg, the same as that for the distributed barrier. The average stone dust concentration was ~3.2 kg/m^3 for the concentrated barrier.

Figure 5.2.5a: Concentrated barrier installation in B-drift

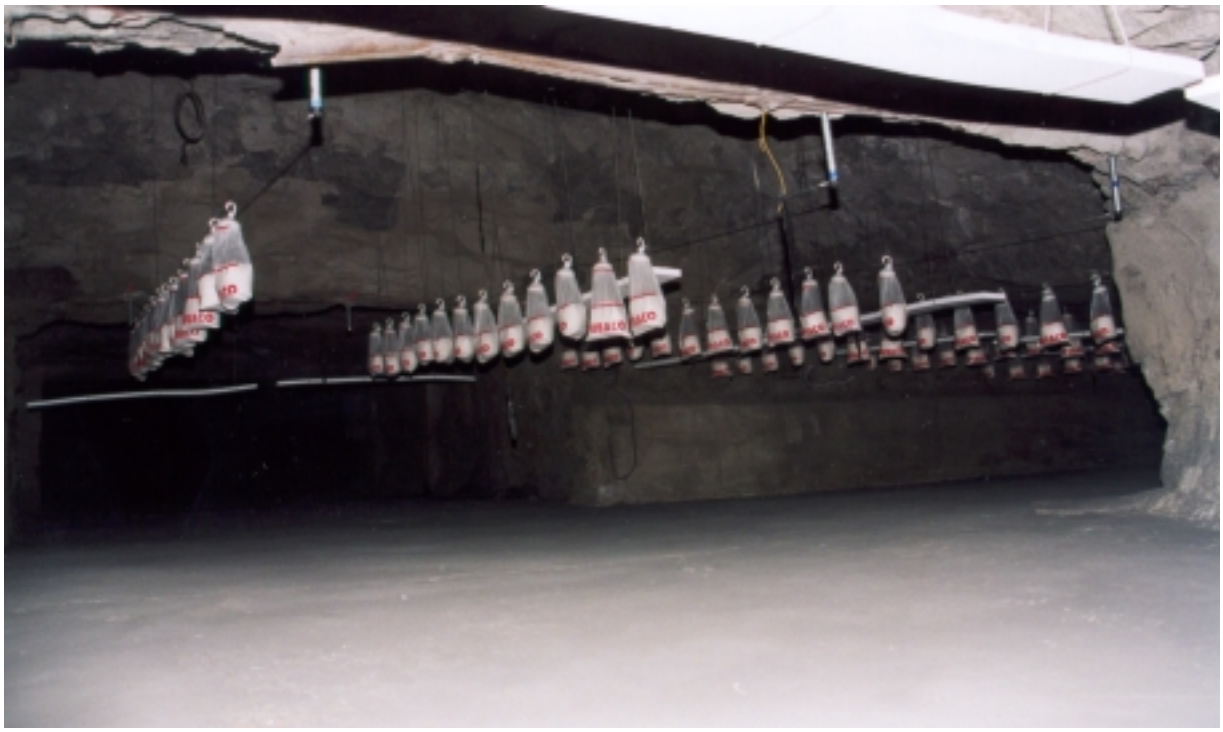

Figure 5.2.5b: Concentrated barrier installation in B-drift, as viewed from the crosscut

5.2.6 Concentrated barrier: LLEM test # 394

The second test to evaluate the performance of the concentrated barrier configuration was similar to the second test (#392) against the distributed barrier configuration. The premixed coal/stone dust was loaded into all three entries; 65% stone dust concentration in B-drift and 80% stone dust concentration in A- and C-drifts. The dusted zone in each entry was 119 m long with the premixed dust distributed half on the suspended roof shelves and half on the entry floor.

The concentrated stone dust barrier was the same as that for the previous test (#393). The stone dust bags were suspended on 16 steel cables from ~74 to ~104 m from the closed end of B-drift. Each steel cable supported 12 bags for a total of 192 bags. The total mass of stone dust was 1152 kg resulting in an average stone dust concentration of 3.2 kg/m^3.

A short summary of all of the baseline and barrier dust explosion tests from Phase II of the project is in Appendix 1b.

5.3 Evaluation methodology

5.3.1 Methane tests evaluation methods

The evaluation of the individual bag performance in Phase I of the project was based on a comparison of the pressures generated by a particular gas explosion and the effect of these pressures on the dispersion efficiency of the bags at various locations in the mine.

The average static pressure for a particular gas explosion was the average of the static pressure measurements recorded from the sensors located just outbye the ignition zone to just inbye crosscut 3. Thus the average static pressure is the arithmetic mean of the following instruments stations: B-2 to B-5 for ignitions in B-drift and C-2 to C-5 for ignitions in C-drift (see Table 3.1).

The operation of the bags against varying dynamic pressure levels is discussed in the following sections. The decay of the dynamic pressure wave away from the ignition source and the effect of the crosscut/entry intersections were also noted.

The performance of each of the individual bags for each test is listed in the appendices, along with the static and dynamic pressures for the test. Figure 5.3.1.3a is a photograph showing a bag that split during the explosion but did not disperse all of the stone dust contained within the bag. Figure 5.3.1.3b is a photograph showing a bag that ruptured and dispersed all its stone dust during the explosion but remained attached to the suspension system. Most bags, including the hook and ring assembly, were fully detached from the mine roof suspension system during the Phase I gas explosions. For each of the bags deployed during an explosion test, the amount of dispersed dust from each was estimated by observing the size of the stone dust pile on the mine floor following the explosion. The estimation of the stone dust pile on the mine floor was categorized as < , , or ½ of the original bag amount. If no pile of dust was observed on the floor, the bag dust was considered to have been fully dispersed. Figure 5.3.1.3c is a photograph showing a technician estimating the stone dust pile outbye the suspended emptied bag following an explosion test.

Figure 5.3.1.3a: Post-explosion photograph of a split bag

Figure 5.3.1.3b: Post-explosion photograph of an emptied bag

Figure 5.3.1.3c: Post-explosion photograph showing an emptied bag still suspended from the mine roof and technician estimating dust deposition on the outbye mine floor

In order to estimate the effectiveness of the bag operation, the following formula was used:

Estimated efficiency of total mass of stone dust dispersed =

Σ (Dispersed mass of stone dust per bag) /(Total mass of stone dust per bag) x 100%

where the dispersed mass of stone dust is estimated by adding the individual bag classifications as follows:

Dust pile	Estimated dispersed dust
0	number of bags x 6 kg
< 1/3	number of bags x 5 kg
1/3	number of bags x 4 kg
1/2	number of bags x 3 kg

The total mass of dust dispersed equals the summation of the number of bags in each category times the estimated stone dust dispersed per bag. For bags that split but did not disperse all of

the stone dust, the split bag with the remaining stone dust was taken outside of the mine and weighed to determine the actual amount of dispersed dust. An estimate of the efficiency of the bags distributed in the individual drifts was calculated by taking only the data of the bags suspended in the specific drift and not the bags suspended in the crosscuts.

5.3.2 Barrier evaluation criteria

Although it is obvious that for a barrier to be considered successful it must "stop" or suppress an explosion, the international literature is more vague as to the precise criterion for when an explosion is considered "stopped" or suppressed. For some people, the barrier is considered successful only if flame propagation is stopped within the barrier zone. Others interpret a barrier system as successful if there is a reduction in the flame travel distance compared to the maximum flame travel distance without a barrier system in place

Du Plessis and Vassard (1997) have proposed two measures of effectiveness for the dispersed barrier evaluation:

1) the explosion can be considered to have "stopped on the spot" if the flame does not progress a distance of more than 25 m beyond the end position of the barrier; and
2) the explosion can be considered to have been "stopped" if the flame propagation is less than it would have been without the barrier.

Because of the finite spacing of the data gathering panels at the LLEM, there was a limitation in judging the exact flame propagation distance. The last flame sensors, as listed in Table 3.1 and shown in Figure 2.1, are located at 198 and 246 m in A-drift, 191 and 238 m in B-drift, and 182 and 231 m in C-drift. In B-drift, this means that the end of the distributed barrier configuration (~170 m from the closed end of B-drift) is approximately 21 m and 68 m, respectively, from the last two flame sensors. However, this limitation did not affect the evaluation of the effectiveness of either the distributed or concentrated barriers, as noted in the results sections of this report.

6 Test Barrier

The barrier configurations evaluated during the NIOSH program were the distributed and the concentrated bagged stone dust barrier configurations.

6.1 Proposed distributed bagged stone dust barrier design

The calculation and the design of the distributed barrier are as follows (Du Plessis, 1997):

a) Assume barrier starts 74 m outbye of the last through road.

b) Protection distance chosen is 100 m

c) Cross-sectional area:

Bord width	=	6,0 m
Height	=	2,0 m (approximately)
Area	=	12,0 m^2

d) Volume of protection area = 12 m^2 x 100 m
= 1 200 m^3

e) Amount of stone dust required:

Q_A	=	12 m^2 x 100 kg/m^2	=	1 200 kg
Q_v	=	1 200 m^3 x 1 kg/m^3	=	1 200 kg

f) Number of bags required:

6 kg/bag	=	1 200/6
	=	200 bags

g) For four sub-barriers:

200/4	=	50 bags/barrier

h) If the outer bags are 0,6 m from the side, 12 bags can be suspended per row, requiring 4 rows of bags per sub-barrier. Assuming the rows of bags are spaced 2,0 m apart and that the ignition position (closed end of B-drift) is the zero position, the sub-barriers will be located at the positions as shown in Table 6.1

Table 6.1

Distributed barrier positions

Distance from face (m)	Description
0	Begin
74 – 80	First sub-barrier
104 – 110	Second sub-barrier
134 – 140	Third sub-barrier
164 – 170	Fourth sub-barrier

CHECK: 48 bags x 4 rows x 6 kg = 1 152 kg

Volume protected = 96 x 12 m²

= 1152 m^3

The stone dust density is 1 kg/m^3 and thus the barrier is correctly designed.

6.2 Proposed concentrated bagged stone dust barrier design

The calculation and the design of the concentrated barrier are shown as follows (Du Plessis, 1997):

a) Cross-sectional area:

Bord width = 6,0 m

Height = 2,0 m (approximately)

Area = 12,0 m^2

b) Amount of stone dust required:

Q_A = 12 m^2 x 100 kg/m^2 = 1 200 kg

c) Number of bags required:

6 kg/bag = 1 200/6

= 200 bags

d) If the outer bags are 0,6 m from the side, 12 bags can be suspended per row, requiring 16 rows of bags for the concentrated barrier configuration. Assuming the rows of bags are spaced 2,0 m apart and that the ignition position (closed end of B-drift) is the zero position, the barrier will be located from 74 to 104 m.

7 Methane test results

The test results (see appendices 2-19) for the baseline explosions as well as the evaluation tests are presented in the following sub-headings.

7.1 Baseline test results

The average static pressures for the various base line explosions are listed in Table 7.1a. As noted earlier in the report, the average static pressures for the gas explosions were calculated from just outbye the first crosscut to just inbye the third crosscut. Note that the average static pressure values listed in Table 7.1a and in Appendix 1a are rounded to the nearest 1 psi and 5 kPa. The detailed peak static and dynamic pressure data at the individual DG panels and instrument stands for the baseline explosion tests are listed in Appendices 2 to 7. Tests #367 to #370 were initiated in C-drift while tests #371 and #372 were initiated in B-drift (see Table 5.1a). As noted earlier in the text, there was an explosion-resistant seal located in the first cross-cut between B- and C-drifts during these tests.

Table 7.1a

Average static pressures

Test	Date	Av. Static Pressure*	
		psi	kPa
#367	13 Jan 99	21	145
#368	22 Jan 99	20	140
#369	27 Jan 99	6	40
#370	1 Febr 99	17	120
#371	5 Febr 99	8	55
#372	10 Febr 99	11	75

Tests #367 and #368 were duplicate baseline 9.5% methane-air ignitions (using the water-filled barrels as turbulence generators) in the 12,2 m long C-drift zone. As listed in table 7.1a, these tests generated similar peak static pressures. For test #370 where the water-filled barrels were removed, a 16% reduction (22.5 kPa) in the average static pressure resulted when compared to the methane ignitions with the barrels in place. Test #369 resulted in a significant pressure reduction due to a shorter gas zone (8,2 m long), reduced gas concentration (8,5%), and the removal of the barrels.

Tests #371 and #372 were for the B-drift ignitions using the 12,2 m long gas zone. As for the C-drift ignitions, there was a reduction (20 kPa or 27%) in the average pressure with the water-filled barrels removed.

Appendices 2-7 list the detailed peak static pressure data as a function of position for the C-drift methane ignitions. The static pressures in C-drift decrease as a function of distance from the ignition source out to data gathering (DG) panel 8 (C-152,7). No clear pattern is evident for the pressure decay in A or B-drift, probably due to the fact that local pressure piling predominates. From the DG 8 position outward, little difference in the static pressure between B- and C-drift is observed. Not all the pressure transducers in A-drift were operational during these tests.

The effect on the peak static pressure in the three entries as a function of distance from the ignition source is shown in Figure 7.1a for tests #367 and #368.

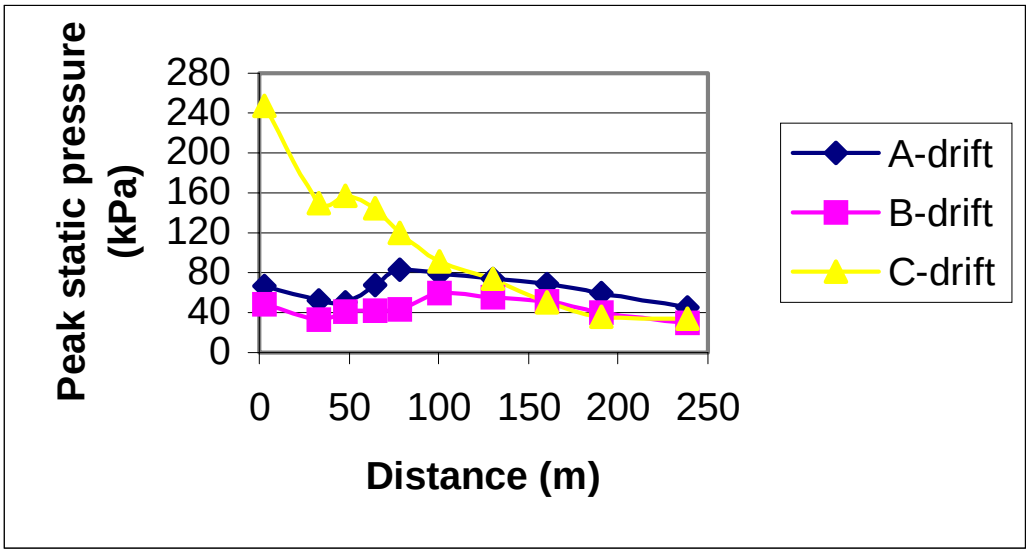

Figure 7.1a: Average static pressure decay for C-drift ignitions

With the gas ignition zone in B-drift, the static pressures in A- and B-drifts were comparable as the explosion resistant seal in crosscut 1 deflected the explosion. Outbye DG 6 (100 m from the closed end of B-drift) little difference in the static pressure for the individual drifts was observed. This decay in the average static pressure for tests #372, #373 and #374 is shown in Figure 7.1b.

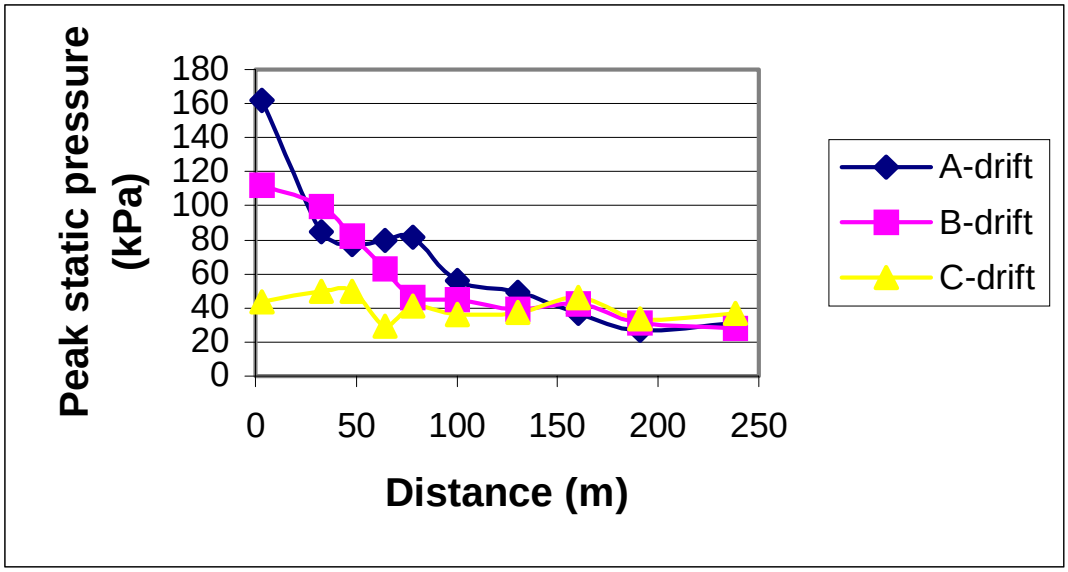

Figure 7.1b: Decay in static pressure as a function of distance outbye the B-drift ignition zone

The rate of static pressure decay is higher for ignitions in B-drift compared with ignitions in C-drift. Presumably, this is due to B-drift having increased venting capabilities to both C-drift and

A-drift whereas C-drift can only vent to B-drift. In general, the static pressures decrease in strength as the distance from the epicentre of the explosion increases. This decline is more pronounced close to the ignition source.

Based on the test results, the average static pressure was influenced by:

- the length of the fuel zone;
- the methane concentration in the fuel-air mixture;
- the presence or absence of the water-filled barrels (turbulence generators); and
- the position of the fuel zone.

Furthermore, the effect of the explosion-resistant seal in crosscut 1 between B- and C-drifts resulted in a gun barrel effect increasing pressures in the drift of the ignition as well as directing the primary pressure wave. This effect should be similar to a shuttle car blocking the one side of the crosscut during the loading phase during normal production.

A summary of the dynamic pressures for the baseline methane ignition tests is listed in Table 7.1b.

Table 7.1b

Dynamic pressure results

Inst. Distance (m)	**Inst. Type**	**Dynamic pressure (kPa)**					
		#367	**#368**	**#369**	**#370**	**#371**	**#372**
B-41	Kistler					31	46
	BDP					29	44
B-73	BDP						17
X-2	BDP			20	55	7	11
C-34	Kistler	Sat*	90	21	75		
	BDP			24	77		
C-64	Kistler	Sat*	86	9	79	2,8	4,1
	BDP			9	79	1,9	2,5

*Note: instrument saturated

The pressure data generated from test #371 (12,2 m long 9,5% methane zone without the barrels in B-drift) corresponded to the definition of a weak explosion (peak static pressure less than 100 kPa with dynamic pressures of 31 kPa at 41 m in B-drift and 3 kPa at 64 m in C-drift). This explosion was used as the weak explosion from B-drift. Baseline test #372 (12,2 m long ~9,5% methane zone with the barrels) corresponded to the definition of the medium explosion from B-drift against which the stone dust bags were evaluated. The strong baseline explosion would be an even longer ignition zone of 21,3 m; i.e. a volume of 146,6 m^3 of 9,5 % methane-air mixture.

7.2 Evaluation of bags: B-drift ignition (with seal)

A total of six explosions were initiated from B-drift with the explosion-resistant seal in crosscut 1 between B- and C-drifts. The detailed test results for tests #373 to #377 are given in Appendices 8 to 19. The average static pressures for the tests are listed in Table 7.2.a, where the last column lists the average pressure for duplicate tests.

Table 7.2a

Average static pressures

Test	Date	Av. Static Pressure		Test Av. Stat. Pressure
		Psi	*kPa*	*kPa*
#373	16 Feb 99	11	*75*	72,5
#374	18 Feb 99	10	*70*	
#375	22 Feb 99	9	*65*	62,5
#378	4 March 99	9	*60*	
#376	25 Feb 99	16	*115*	110
#377	3 March 99	15	*105*	

The increase in the methane-air volume from 146,6 m^3 to 256 m^3 (tests #373 and 374 compared with tests #376 and #377) resulted in an increase of 37,5 kPa in the average static pressure. The removal of the water-filled barrels in the methane zone (tests #375, #377, and #378) decreased the average static pressure by about 10 kPa.

The dynamic pressure data for the B-drift methane ignition tests at the various sensor locations are listed in Table 7.2b. The listed dynamic pressure values were determined from the first observed pressure peak, even though the second or later peak may have been higher.

Table 7.2b

Peak dynamic pressures

Instr. Distance (m)	Instr. Type	Dynamic pressure (kPa)					
		#373	#374	#375	#376	#377	#378
A-49	BDP	21	--	21	74	55	25
A-79	BDP	20	20	17	41	37	19
B-41	Kistler	49	44	37	112	73	32
	BDP	46	42	36	101	--	--
B-73	BDP	18	16	14	46	27	11
B-101	BDP	--	--	--	--	20	8
X-2	BDP	11	10	9	33	18	7
C-64	Kistler	3,9	3,7	3,1	6,5	4,6	2,6
	BDP	3,6	3,2	2,7	4,8	3,9	1,8

The presence of the water-filled barrels in the 12,2 m fuel zone (tests #373 and #374) compared to (tests #375 and #378) increased the average dynamic pressure from ~34 kPa to ~45 kPa at platform B-41 and from 12,5 kPa to 17 kPa at platform B-74. As it was planned to install the first barrier just outbye position B-2, all the 12,2 m methane zone explosions can be considered as weak (< 20 kPa peak dynamic pressure).

The installation of a bi-directional probe (BDP) at 101 m in B-drift aided in defining the pressure decay as a function of distance from the ignition source. In Figure 7.2, the decays in the dynamic pressure for test #377 and test #378 are shown. In test #377 with a 21,3 m long 9,5% methane ignition zone, the dynamic pressure decay with distance was much more rapid than was observed for test #378 which used a 12,2 m long 9,5% methane ignition zone. This pressure decay rate was a function of explosion pressure strength; for lower pressure level explosions, little pressure decay was observed.

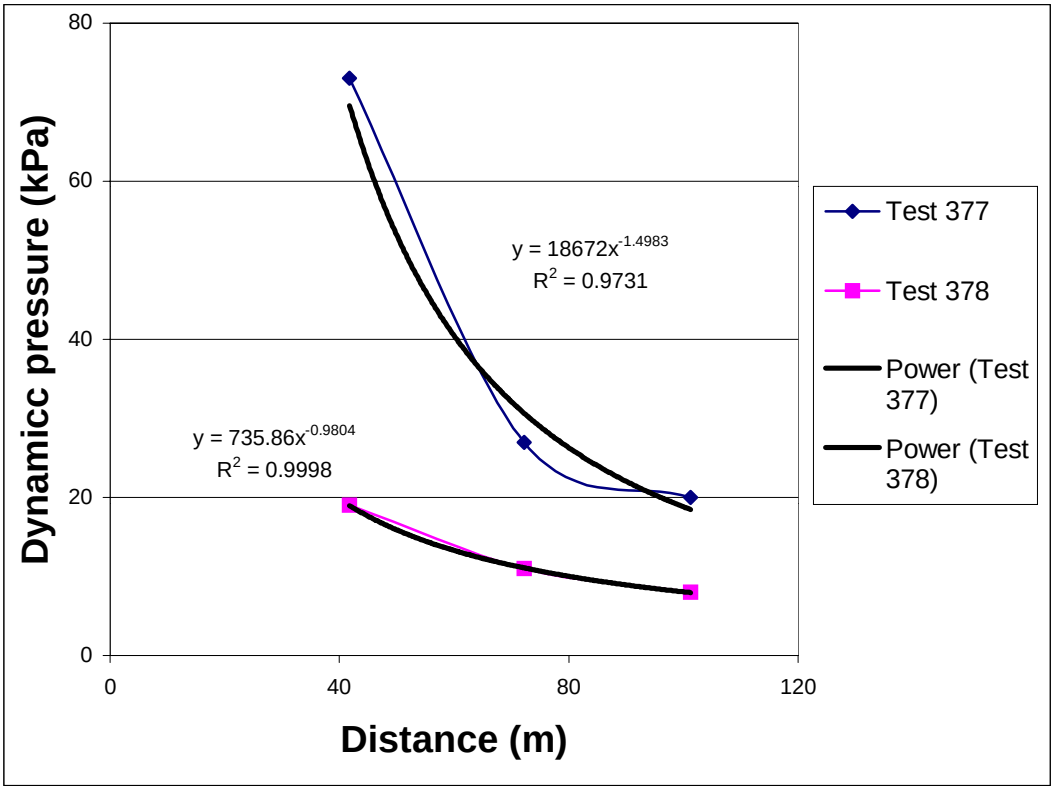

Figure 7.2: Dynamic pressure decay as a function of distance from the ignition source

A summary of the stone dust distribution efficiency for the various explosions and conditions is shown in Table 7.2c. The listed percentages are the estimated percent of the total dust in the bags that was dispersed efficiently. The "total efficiency" listed in column two is the efficiency of all of the bags, including those in both the drifts and the cross-cuts. The "drift efficiency" listed in column three is the efficiency of only the bags located in the drifts. The last three columns list the efficiency of dispersion from the bags in individual drifts.

Table 7.2c

Stone dust distribution efficiency estimate: B-drift ignition with seal

Test	Total eff. (%)	Drift eff. (%)	Drift A Eff. (%)	Drift B Eff. (%)	Drift C Eff. (%)
#373	59	75	69	79	63
#374	59	67	75	80	43
#375	54	70	79	67	75
#378	58	64	88	60	45
#376	72	90	93	93	83
#377	72	89	97	96	67

As can be seen in Table 7.2c, the efficiency of operation of the bags was generally higher in the direction of the primary explosion wave. Furthermore, the operation of the bags in the crosscuts was far less efficient. This can be attributed to the effect of pressure equalization in between the individual drifts as well as the presence of the seal in crosscut 1 which influenced the direction of the pressure waves.

In general, it was observed during the LLEM program that the stronger the explosion strength, the higher the dust distribution efficiency. For ignitions in B-drift, the stone dust distribution in C-drift is less than in A- and B-drift; this is partially attributed to the effect of the seal in crosscut 1.

7.3 Evaluation of bags: B-drift ignition (without seal)

The detailed test results for tests #383 and #384 are given in Appendices 18 and 19. The calculated average static pressures for tests #383 and #384 are shown in Table 7.3a.

Table 7.3a

Average static pressures: B-drift ignition without seal

Test	Date	Av. Static Pressure*	
		psi	Kpa
#383	31 March 99	10	70
#384	4 Feb 99	16	110

With all else essentially being equal, increasing the length of the fuel zone from 12,2 m to 21,3 m (increase in the methane-air volume from 146 m^3 to 256 m^3) resulted in an increase in the average static pressure from 70 to 110 kPa (~57% increase). These pressures are similar to those in the tests with the explosion-resistant seal in crosscut 1 (see Table 7.2.a).

The peak dynamic pressure data for tests #383 and #384 are listed in Table 7.3b.

Table 7.3b

Peak dynamic pressures

Instr. Distance (m)	Instr. Type	Dynamic pressure (kPa)	
		#383	#384
A-49	BDP	15	64
B-41	Kistler	39	88
B-73	BDP	14	32
B-101	BDP	11	19
X-2	BDP	8	19
C-34	BDP	8	18
C-64	Kistler	13	29

The removal of the seal in crosscut 1 (compare Table 7.3b with Table 7.2b) resulted in a reduction in the measured dynamic pressures in B-drift (between 4 and 6 kPa) and A-drift (6 kPa), but an increase in the dynamic pressures in C-drift. This increase of the dynamic pressures in C-drift is the net result of the pressure equalization. The decay in the dynamic pressure wave in B-drift is shown in Figure 7.3.

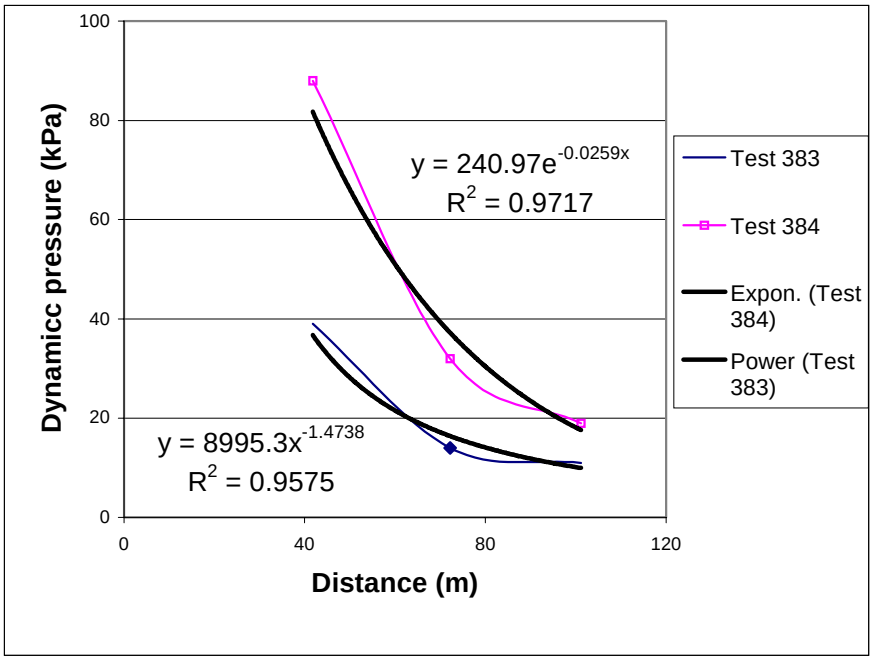

Figure 7.3: Dynamic pressure decay in primary explosion direction

A rapid reduction in the dynamic pressure occurs as the distance from the ignition source increases. The data in Figure 7.3 are similar to those in Figure 7.2 in that there is a more rapid decay in the dynamic pressure for the stronger explosion (test #384).

The stone dust distribution for the tests conducted without a seal in crosscut 1 is shown in Table 7.3c.

Table 7.3c

Stone dust distribution: B-drift ignition without seal

Test	Total eff. (%)	Drifts eff. (%)	Drift A Eff. (%)	Drift B Eff. (%)	Drift C Eff. (%)
#383	55	75	70	82	60
#384	65	85	83	94	70

The stone dust distribution is the highest in the direction of the primary explosion pressure pulse, i.e., in B-drift. The stone dust distribution in A-drift is higher than in the stone dust distribution in C-drift. There is no clear explanation for this phenomenon.

The removal of the seal in crosscut 1 resulted in a reduced total mass distribution efficiency. The efficiency of the individual drifts is comparable. This indicates an increased effect of pressure equalisation on the bags resulting in a reduced stone dust distribution in the crosscut positions.

It was further observed that the stone dust bag suspended just outbye of the methane zone (position 29) operated effectively. The time delay between the methane flame and the dynamic pressure wave arriving at the position of the first platform and the position of the bag was 50 ms (calculated for test #383). This indicates that the bag will operate effectively at a time interval of approximately 50 ms during the high-pressure explosions.

7.4 Evaluation of bags: C-drift ignition (with seal)

The detailed results for tests #379 and #380 (both with a 14,3 m long 9,5% methane-air zone in C-drift) are given in Appendices 14 and 15. The calculated average static pressures for tests #379 (no barrels) and #380 (with barrels) are listed in Table 7.4a.

Table 7.4a

Average static pressures: C-drift ignition with seal

Test	Date	Av. Static Pressure*	
		Psi	*kPa*
#379	8 March 99	18	*120*
#380	10 March 99	17	*120*

In test #380, the addition of the barrels did not increase the average static pressure. Both the explosions can be classified as being strong explosions (static pressure greater than 100 kPa)

The peak dynamic pressures for #379 and #380 are listed in Table 7.4b.

Table 7.4b

Peak dynamic pressures

Instr. Distance (m)	Instr. Type	Dynamic pressure (kPa)	
		#379	#380
A-49	BDP	-6	-6
A-79	BDP	5	4
B-41	BDP	-7	-5
B-73	BDP	8	6
B-101	BDP	12	14
X-2	BDP	57	50
C-34	Kistler	-	-
C-64	Kistler	87	73

The negative values in the table denote dynamic pressures in the direction of the A- and B-drift faces rather than away from the faces. These negative dynamic pressures occurred at the A- and B-drift instrument platforms closest to the face, between crosscuts 1 and 2. The seal, located in crosscut 1 between B- and C-drifts, prevented the pressure wave from the C-drift methane ignition from traveling into B- and A-drift until the pressure wave reached the open crosscut 2. At this point, the pressure wave traveled back toward the faces (closed ends) of B- and A-drifts resulting in the negative dynamic pressures. The seal in crosscut 1 also resulted in an extremely strong pressure wave traveling down C-drift with much lower pressures measured in A- and B-drifts.

Table 7.4c

Stone dust distribution: C-drift ignition with seal

Test	Total eff. (%)	Drift eff. (%)	Drift A eff.(%)	Drift B eff. (%)	Drift C eff.(%)
#379	73	76	60	72	100
#380	71	76	50	74	90

A high stone dust dispersal efficiency was achieved during the C-drift methane ignitions with the seal was in place. The least efficient bag operations were in A-drift being that the bags in this entry were furthest away from the ignition source and, therefore, were subjected to lower pressures.

7.5 Evaluation of bags: C-drift ignition (without seal)

The detailed results for tests #381 and #382 (both with a 14,3 m long 9,5% methane-air zone in C-drift) are given in Appendices 16 and 17. Table 7.5a lists the average static pressures for tests #381 (with barrels) and #382 (no barrels).

Table 7.5a

Average static pressure: C-drift ignition without seal

Test	**Date**	**Av. Static Pressure***	
		Psi	***kPa***
#381	24 March 99	12	85
#382	26 March 99	9	65

In these tests, the use of water-filled barrels did influence the average static pressure; an average static pressure of 85 kPa with the barrels compared with 57 kPa without the barrels. As would be the expected outcome, a comparison of similar tests with (120 kPa for #380) and without (85 kPa for #381) the seal in crosscut 1 revealed a marked reduction of the static pressures.

The peak dynamic pressures for the C-drift explosions are shown in Table 7.5b.

Table 7.5b

Peak dynamic pressures

Instr. Distance (m)	Instr. Type	Dynamic pressure (kPa)	
		#381	#382
A-49	BDP-1	8	6
A-79	BDP-3	15	13
B-41	BDP-2	16	12
B-73	BDP-4	17	10
B-101	BDP-6	18	11
X-2	BDP-5	17	11
C-34	Kistler	50	33
C-64	Kistler	*	16

*Kistler disk was broken during test

In these tests, the dynamic pressure pulse equalizes quickly with most of the peak dynamic pressures being similar in all drifts independent of the distance from the ignition source. The measured pressures in B-drift at each of the three platform locations are almost equal. If this is compared to the data in the same drift (C) as the ignition, a marked difference is observed.

Table 7.5c

Stone dust distribution: C-drift ignition without seal

Test	Total eff. (%)	Drift eff. (%)	Drift A eff. (%)	Drift B eff. (%)	Drift C eff. (%)
#381	61	70	63	74	70
#382	61	74	67	67	93

The removal of the seal in crosscut 1 resulted in a decrease of more than 10% in the total mass efficiency of the operation of the bags if compared to the previous tests in C-drift where the seal was in place.

8 Coal dust explosion test results

8.1 Coal dust baseline test results

8.1.1 Baseline test 1: LLEM test #389

The first baseline static pressure test results for the various drifts are listed in Table 8.1.1a.

Table 8.1.1a

Peak static pressures for LLEM test #389

Drift A		Drift B		Drift C	
Instr. Pos.	**Pressure (kPa)**	**Instr. Pos.**	**Pressure (kPa)**	**Instr. Pos.**	**Pressure (kPa)**
A1	--	B1	194	C1	181
A2	163	B2	166	C2	97
A3	117	B3	186	C3	126
A4	108	B4	93	C4	95
A5	84	B5	80	C5	83
A6	69	B6	63	C6	67
A7	63	B7	61	C7	59
A8	--	B8	57	C8	59
A9	--	B9	47	C9	55
A10	--	B10	42	C10	50

This baseline coal and stone dust explosion test #389 had an 82 m long zone in B-drift of premixed coal and stone dust at 65% stone dust or 68% TIC. There were no dust zones in A- or C-drifts. The average static pressure from B2 to B8 for LLEM #389 was ~100 kPa in B-drift, with slightly lower average static pressures in A- and C-drifts. The average static pressure from B2 to B5 was ~130 kPa, considerably higher than the ~110 kPa for the gas

ignition zone without any coal dust (LLEM #384 in Table 7.3a). The decay in the static pressure for the various drifts is shown in Figure 8.1.1a.

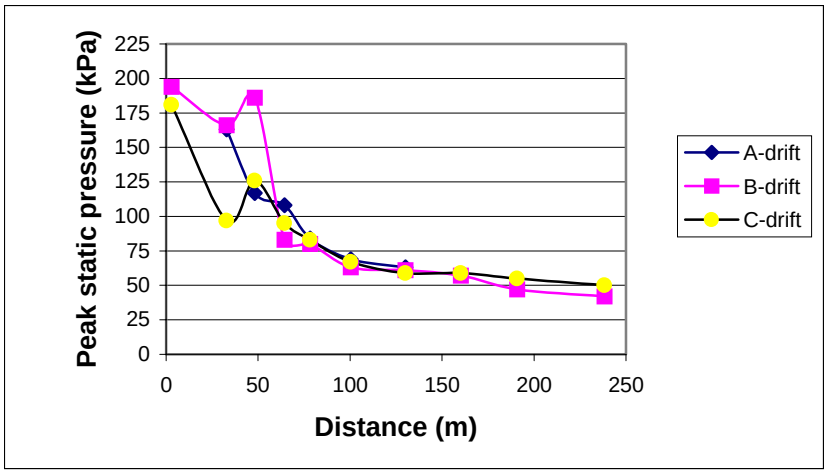

Figure 8.1.1a: Static pressure decay for LLEM Test #389

The peak dynamic pressures for LLEM test #389 are listed in Table 8.1.1b**.**

Table 8.1.1b

Peak dynamic pressures LLEM test #389

Instr. Distance (m)	Instr. Type	Dynamic pressure (kPa)	Av. Dynamic Pressure (kPa)
A-49	BDP	65	65
C-34	BDP	32	32
B-41	BDP	121	121
B-73	Kistler	44	
	BDP	38	41
B-101	Kistler	33	
	BDP	17	25
B-130	BDP	16	16

In a 90 m (spanning three intersections) distance in B-drift, the dynamic pressure reduced from 121 kPa to 16 kPa.

For this baseline test, the flame traveled ~160 m from the face of the methane ignition zone in B-drift. The flame also went into cross-cuts 1 through 4, and reached the second and third flame sensors in A- and C-drifts. The detailed flame sensor data are in appendix 20. In addition to the electronic flame sensors, strips of thin plastic were hung from the roof throughout the multiple entry. The last recorded flame position would still have been within the planned zone for the distributed barrier. Therefore, a longer coal dust zone was needed for the baseline test.

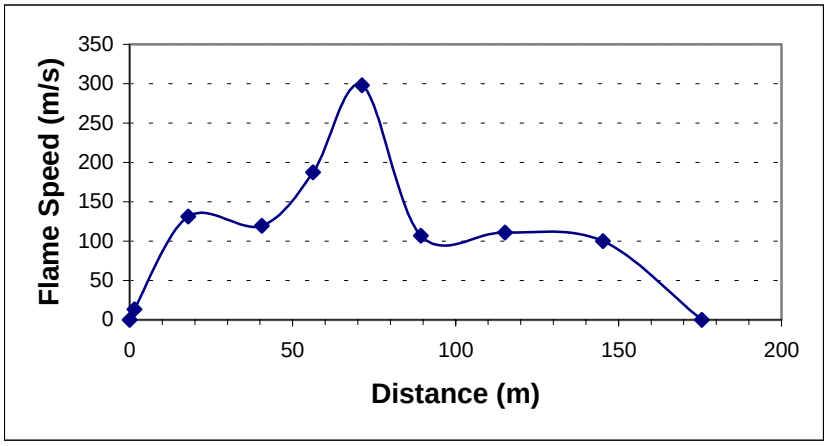

Figure 8.1.1b: Flame speed in B-drift for LLEM test #389

The flame speed in B-drift is shown in Figure 8.1.1b. The maximum flame speed of 298 m/s was calculated at 71 m from the ignition source. At the proposed position of the first sub barrier starting at 74 m from the closed end of B-drift, the calculated flame speed was ~262 m/s. The flame speeds at the positions that will be used for the other sub-barriers were 109 m/s for the second (101 m) and 104 m/s for the third (131 m). No flame was observed at the proposed position of the fourth sub barrier (162 m) during this test.

The temperature calculated from the heat flux data was ~1560 C at B-64 and ~1410 C at B-100.

The time delay between the peak dynamic pressure and flame arrival was calculated at the dynamic pressure sensor position through interpolation of the flame and dynamic pressure sensor data to coincide with the dynamic pressure sensor position. The mean delay times are:

First sub-barrier	148 ms
Second sub-barrier	180 ms
Third sub-barrier	406 ms

The flame did not reach the fourth sub barrier position. This indicates the minimum time of 148 ms at the first sub barrier position for the stone dust bags to disperse to effectively inhibit the flame propagation.

8.1.2 Baseline test 2: LLEM test #390

A second baseline test was conducted with a longer dusted zone (119 m long) in order to extend the flame to well beyond the final sub-barrier position. The second baseline static pressure test results for the various drifts are shown in Table 8.1.2a.

Table 8.1.2a

Peak static pressures for LLEM test #390

Drift A		Drift B		Drift C	
Instr. Pos.	**Pressure (kPa)**	**Instr. Pos.**	**Pressure (kPa)**	**Instr. Pos.**	**Pressure (kPa)**
A1	-	B1	183	C1	200
A2	121	B2	186	C2	124
A3	124	B3	179	C3	131
A4	124	B4	104	C4	-
A5	104	B5	100	C5	86
A6	76	B6	72	C6	79
A7	69	B7	62	C7	69
A8	69	B8	62	C8	69
A9	-	B9	49	C9	62
A10	59	B10	48	C10	61

The average static pressure (from B2 to B8) for this second baseline dust explosion was ~110 kPa, with comparable or slightly lower average static pressures in A- and C-drifts. The decay in the static pressure for the various drifts is shown in Figure 8.1.2a.

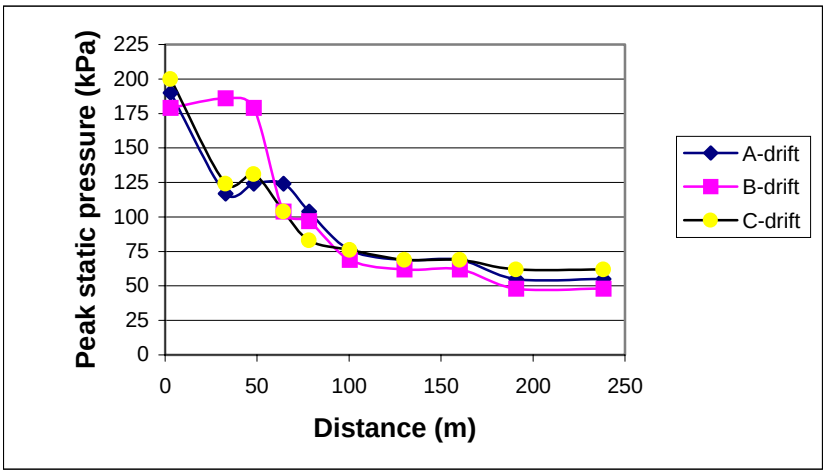

Figure 8.1.2a: Static pressure decay for LLEM test #390

The peak dynamic pressures were not recorded due to a 1 s triggering delay malfunction on the PC-DAS data acquisition system (bad connection on the triggering system).

The flame extended to ~250 m in B-drift, and into cross-cuts 1 through 5 toward A-drift and into cross-cuts 1 to 4 toward C-drift. The flame speed in B-drift is shown in Figure 8.1.2b.

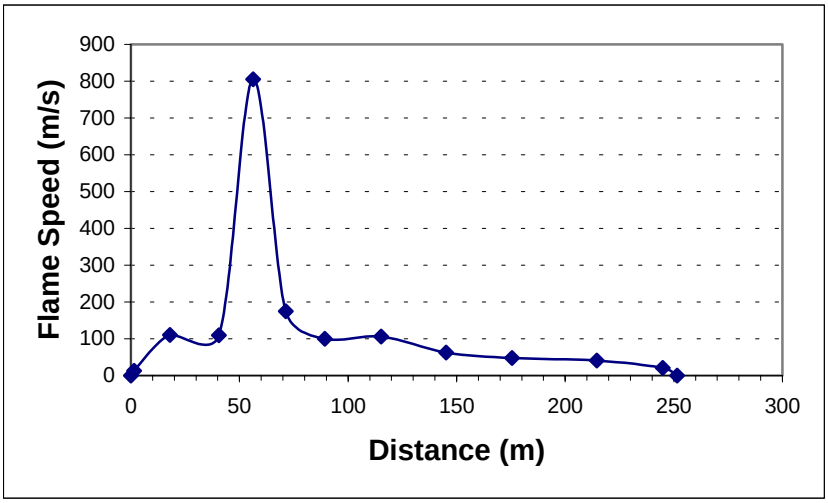

Figure 8.1.2b: Flame speed in B-drift for LLEM test # 390

The maximum flame speed was calculated at 805 m/s at 56 m flame sensor. At 74 m from the closed end of B-drift (the position where the first sub barrier will be located), the calculated flame speed was ~161 m/s. At the positions where the other sub barriers will be located, the calculated flame speeds were 104 m/s for the second, 80 m/s for the third and 54 m/s for the fourth sub barrier. The average flame speed was 102 m/s.

The temperatures were ~1470 C at B-64 and ~1370 C at B-100. The detailed data from these and all the other sensors are in Appendix 21.

The time delay between the peak dynamic pressure and flame arrival was calculated at the dynamic pressure sensor position through interpolation of the flame and pressure sensor data. To estimate the time delay at the sub barrier positions it was assumed that the peak static pressure coincided with that of the peak dynamic pressure as no data was captured as previously described. The peak static pressure time was interpolated at the first sub barrier position. The times at the peak pressure for the other sub barrier positions were used to estimate the time delay between flame arrival and pressure at the beginning position of each of the sub barriers. The mean delay times (Δt) are shown below.

First sub barrier	132 ms
Second sub barrier	320 ms
Third sub barrier	450 ms
Fourth sub barrier	880 ms

This provides a minimum time of 132 ms (the flame arrival at the first sub barrier position) for the stone dust bags to disperse for effective inhibition of the flame propagation.

8.2 Distributed bagged barrier test results

8.2.1 Distributed barrier test: LLEM test #391

Test #391 was a repeat of baseline test #390, except that the distributed barrier was installed in B-drift. The static pressure test results for the various drifts are listed in Table 8.2.1a.

Table 8.2.1a

Peak static pressures for LLEM test #391

Drift A		Drift B		Drift C	
Instr. Pos.	**Pressure (kPa)**	**Instr. Pos.**	**Pressure (kPa)**	**Instr. Pos.**	**Pressure (kPa)**
A1	-	B1	201	C1	177
A2	146	B2	174	C2	120
A3	131	B3	168	C3	128
A4	113	B4	86	C4	110
A5	90	B5	90	C5	79
A6	69	B6	65	C6	66
A7	68	B7	63	C7	66
A8	65	B8	59	C8	63
A9	59	B9	48	C9	59
A10	52	B10	45	C10	53

The average static pressure for B2 to B8 was ~100 kPa. The decay in the static pressure for the various drifts is shown in Figure 8.2.1a.

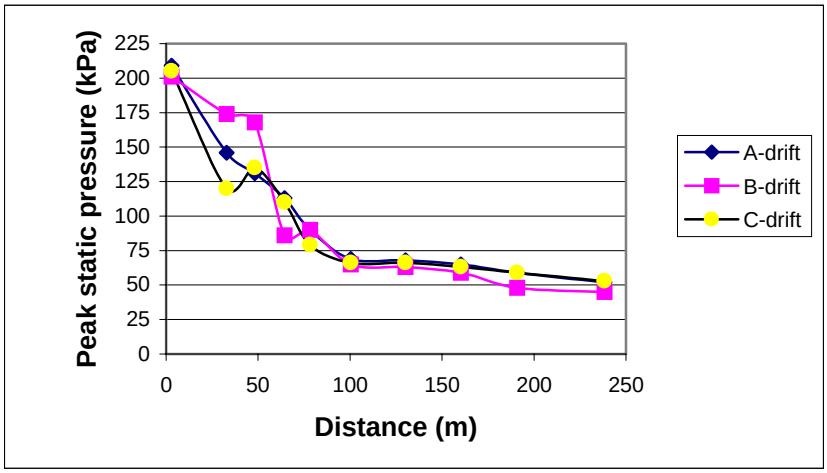

Figure 8.2.1a: Static pressure decay for LLEM test #391

As evidenced in Figure 8.2.1a, the pressure equalisation in the three drifts is much quicker than for that observed in the methane only tests. The pressure in each of the three drifts is nearly equal by 60 m outbye the ignition position; only 40 m beyond the end of the methane zone.

The peak dynamic pressures for LLEM test #391 are listed in Table 8.2.1b**.** The listed values are for the first peaks at the various locations, even though the second peak may have been higher.

Table 8.2.1b

Peak dynamic pressures for LLEM test #391

Instr. Distance (m)	Instr. Type	Dynamic Pressure (kPa)	Av. Dynamic Pressure (kPa)
A-49	BDP	66	66
C-34	BDP	24	24
B-41	Kistler	150	138
B-41	BDP	116	
B-73	Kistler	76	70
	BDP	63	
B-101	BDP	20	20
B-130	BDP	5	5

The dynamic pressure reduced from 138 kPa to 5 kPa over a 90 m distance (spanning three intersections). The B-73 Kistler probe was damaged during this test. The dynamic pressure at the first three sub barrier positions were:

- First sub barrier position 70 kPa
- Second sub-barrier position 20 kPa
- Third sub-barrier position 5 kPa

The flame extended only to ~100 m in B-drift, with flame into the first three cross-cuts toward A-drift and into the first two cross-cuts toward C-drift. The flame only extended to the beginning of the second sub barrier indicating extinguishment of the propagating flame within 30 m of the first sub barrier. The total flame reduction was approximately 150 m in B-drift.

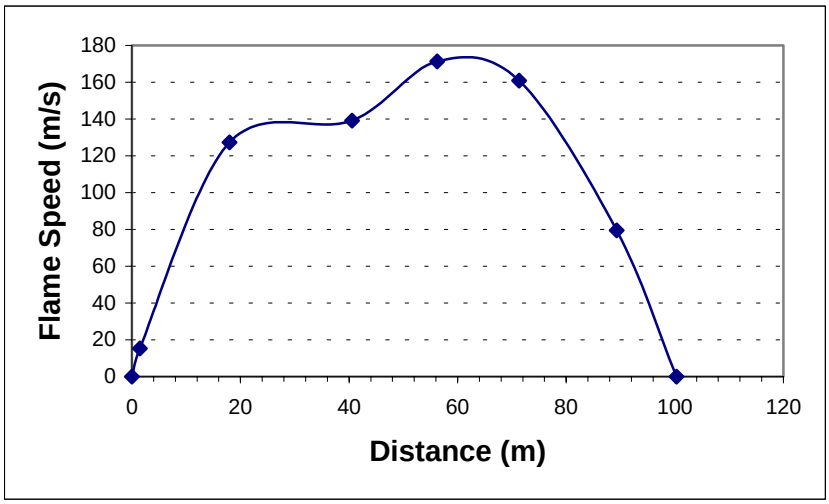

Figure 8.2.1b: Flame speed in B-drift for LLEM test #391

The flame speed in B-drift is shown in Figure 8.2.1b. The flame reached a maximum flame speed of 171 m/s at 56 m. At the position of the first sub barrier, the flame speed was calculated as 145 m/s. The flame speed significantly decreased until such time as it was quenched near the beginning of the second sub-barrier.

The calculated temperature was 1540 C at B-64. There was no heat flux measured at the second barrier position because there was no flame.

The time delay (Δt) between the peak dynamic pressure and flame arrival was calculated at the dynamic pressure sensor position through interpolation of the flame sensor data to coincide with the dynamic pressure sensor position. The mean delay time at the first sub barrier position was 166 ms. This is an indication of the minimum time available for the stone dust bags to disperse the stone dust effectively to inhibit further flame propagation.

Stone dust distribution was excellent for all the sub barriers with only three bags found with limited amounts of stone dust inside them. These bags were found outby the last sub barrier position

No barrier bags, bag remnants, or hooks remained on the cables suspending the bags in the first three sub barriers following the explosion test. In the fourth sub barrier, 4 hooks and bags remained on the cables. The bags showed the classic mode of operation; i.e., vertical shredding

or tearing of the plastic. Approximately 14 kPa of dynamic pressure was exerted on the bags at this fourth sub barrier position. Bag remains, stone dust, and polystyrene shelving debris were found in all three entries well beyond the last sub barrier position.

8.2.2 Distributed barrier test: LLEM test #392

In test #392, the dust was loaded in all three entries. In A and C-drifts, the 119 m long premixed coal/stone dust zone contained 80% stone dust with a coal concentration of 150 g/m^3. In B-drift, 119 m long premixed coal/stone dust zone contained 65% stone dust at the same coal concentration. The distributed barrier was installed in B-drift, the same as for test #391. The static pressure test results for the various drifts are shown in Table 8.2.2a.

Table 8.2.2a

Peak static pressures for LLEM test #392

A drift		B drift		C drift	
Instr. Pos.	**Pressure (kPa)**	**Instr. Pos.**	**Pressure (kPa)**	**Instr. Pos.**	**Pressure (kPa)**
A1	156	B1	148	C1	151
A2	95	B2	129	C2	92
A3	84	B3	122	C3	97
A4	77	B4	81	C4	86
A5	66	B5	77	C5	70
A6	69	B6	70	C6	66
A7	60	B7	51	C7	56
A8	54	B8	46	C8	45
A9	51	B9	43	C9	48
A10	45	B10	41	C10	47

The average static pressure for B2 to B8 in B-drift was ~80 kPa. The decay in the static pressure for the various drifts is shown in Figure 8.2.2a.

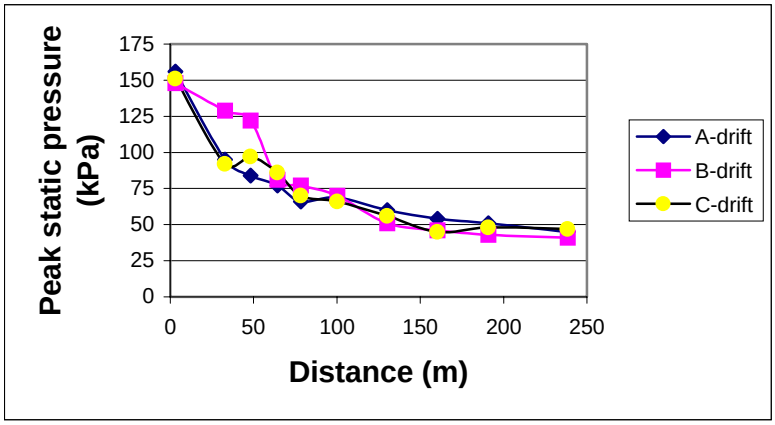

Figure 8.2.2a: Static pressure decay for LLEM test #392

The peak dynamic pressure for LLEM test #392 is shown in Table 8.2.2b**.**

Table 8.2.2b

Peak dynamic pressures for LLEM test #392

Instr. Distance (m)	Instr. Type	Dynamic Pressure (kPa)	Av. Dynamic Pressure (kPa)
A-49	BDP	31	31
C-34	BDP	19	19
B-41	BDP	120	120
B-73	Kistler	*	44
	BDP	44	
B-101	BDP	13	13
B-130	BDP	3	3

*Kistler probe was damaged during test.

The dynamic pressure in B-drift reduced from 120 kPa to 3 kPa over a 90 m distance which spanned three intersections.

The flame extended to ~150 m in B-drift, with flame into the first four cross-cuts toward A- and C-drifts. The flame extended beyond the position of the third sub barrier but not beyond the

fourth sub barrier position, indicating extinguishment of the propagating flame within 75 m of the start of the first sub barrier. The total flame reduction was ~100m in B drift. For both LLEM test #392 and test #391, the barriers were successful in stopping flame propagation within the barrier zone, even though the flame traveled further for the test (#392) with coal dust in all three entries.

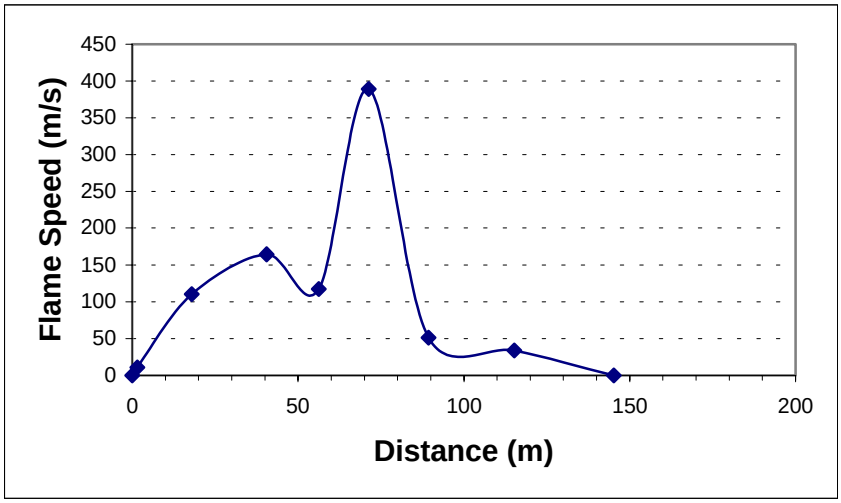

Figure 8.2.2b: Flame speed in B-drift for LLEM test #392

The flame speed in B-drift is shown in Figure 8.2.2b. A sharp increase in the flame speed was observed as the flame reached the first sub barrier position. A maximum flame speed of 389 m/s at 71 m (just in front of the first sub barrier position) was calculated. The flame speed rapidly decreased to approximately 51 m/s approaching the second sub barrier position and 34 m/s approaching the third sub barrier position. The flame was finally quenched ~14 m beyond the outbye position of the third sub barrier.

The temperature calculated was ~1630 C at B-64; the instrument at the second barrier position malfunctioned.

The time delay between the peak dynamic pressure and flame arrival was calculated at the dynamic pressure sensor position through interpolation of the flame sensor data to coincide with the dynamic pressure sensor position. The mean delay time (Δt) between the flame arrival and dynamic pressure peak value is given below:

- 158 ms at the first sub barrier position;

- 539 ms at the second sub barrier position; and
- 1346 ms at the third sub barrier position.

The time available for the stone dust bags to disperse the stone dust effectively prior to the flame arrival at the first sub barrier position was only slightly less the time required in test #391 (B-drift only dust loading). As for test #391, there were a few hooks and parts of bags remaining on the cables in the fourth sub-barrier (Figure 8.2.2c).

Figure 8.2.2c: Photograph of remnants of bags at the fourth sub-barrier

The differences in the flame speeds between the tests (#391 and #392) could be related to the added fuel zones in A- and C-drifts for test #392, which may have acted as a channel effect, increasing the flame speeds and flame propagation rate in B-drift. Another contributing factor which may have influenced the differences in the flame speeds was the final concentration of methane in the gas zone prior to initiation (1.7 m^3 of additional natural gas was added during test #392 compared to test #391). The increase in the fuel (coal dust) available for combustion in B-drift from the dust loadings in A- and C-drifts may have also contributed to the slightly faster flame speeds during test #392. However, the flame in B-drift beyond the first sub barrier position during test #392 was barely propagating and can be

described as a wandering flame. The flame observed in A- and C-drifts cannot be classified as a propagating explosion, but should be considered rather as combustion of coal that was ignited by the flame extending through the cross-cuts from B-drift. This was confirmed by the flame sensor time-plots for A- and C-drifts, which showed that the flame arrived later in A- and C-drifts than in B-drift.

It can be concluded that the distributed barrier effectively stopped the coal dust explosion flame propagation within the barrier although the flame extended an additional 50 m in test #392, compared to the results of the test 391, where there was coal dust only in B-drift.

8.3 Concentrated bagged barrier test results

Two coal dust explosion evaluation tests were conducted against the concentrated barrier, which was installed in B-drift. The two evaluation tests were analogous to the two tests (#391 and #392) for the distributed barrier. The first test (#393) was conducted with the premixed 68% TIC coal/stone dust zone only in B-drift; the second test (#394) also had this same B-drift dust zone with the addition of 82%t TIC dust zones in A- and C-drifts.

8.3.1 Concentrated barrier test: LLEM test #393

The first test (#393) against the concentrated barrier configuration utilized the same ignition zone and dust zone as the baseline test #390 and the first test (#391) against the distributed barrier (21,3 m long 9,5% methane ignition zone with a 119 m long 68% TIC dust zone). The peak static pressure test results for the various drifts are shown in Table 8.3.1a.

Table 8.3.1a

Peak static pressures for LLEM test #393

A drift		B drift		C drift	
Instr. Pos.	**Pressure (kPa)**	**Instr. Pos.**	**Pressure (kPa)**	**Instr. Pos.**	**Pressure (kPa)**
A1	190	B1	203	C1	199
A2	145	B2	184	C2	118
A3	119	B3	162	C3	133
A4	111	B4	106	C4	112
A5	72	B5	94	C5	78
A6	69	B6	63	C6	70
A7	70	B7	61	C7	60
A8	61	B8	58	C8	59
A9	57	B9	47	C9	61
A10	51	B10	45	C10	55

The average peak static pressure for B-drift was ~105 kPa. The decay in the static pressure for the various drifts is shown in Figure 8.3.1a.

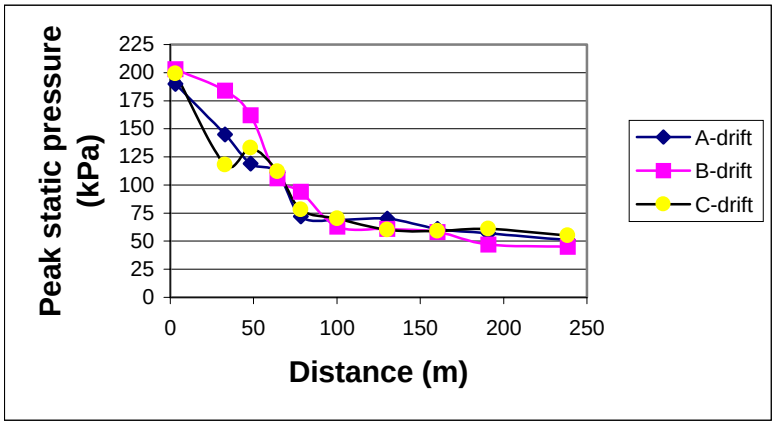

Figure 8.3.1a: Static pressure decay for LLEM test #393

Table 8.3.1b

Peak dynamic pressures for LLEM test #393

Instr. Distance (m)	Instr. Type	Dynamic Pressure (kPa)	Av. Dynamic Pressure (kPa)
A-49	BDP	57	57
C-34	BDP	28	28
B-41	BDP	123	123
B-73	Kistler	47	53
	BDP	59	
B-101	BDP	2	2
B-130	BDP	3	3

The peak dynamic pressure for LLEM test #393 is shown in Table 8.3.1b. As for the previous dynamic pressure data, the listed values in the table are for the first peaks at the various locations, even though the second peak may have been higher. The dynamic pressure in B-drift reduced from 123kPa to 3 kPa over an 89 m distance which spanned three intersections.

The flame extended to ~95 m in B-drift, with flame into the first three cross-cuts toward A-drift and into the first two cross-cuts toward C-drift. Flame propagation was stopped within the barrier and the flame extended less than 20 m from the barrier start position. The total flame reduction when compared with the baseline dust explosion test #390 (B-drift dust loading only) was approximately 155 m in B-drift. Less flame was recorded in A- and C-drifts compared to the baseline test due to the reduction of the flame in B-drift.

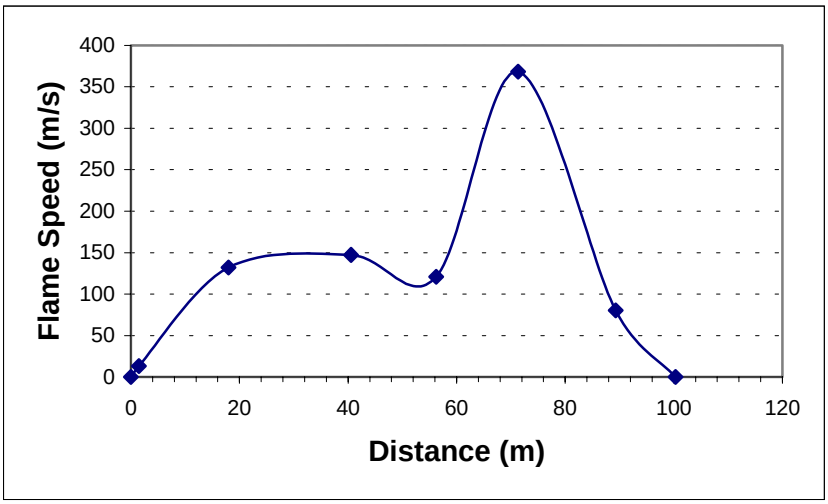

Figure 8.3.1b: Flame speed in B drift for LLEM test #393

The flame speed in B-drift is shown in Figure 8.3.1b. The flame reached a maximum flame speed of 368 m/s at 71 m. At the position of the first sub-barrier, the flame speed was calculated as 314 m/s. The flame speed decreased rapidly within the concentrated barrier zone and was quenched well within the barrier zone.

The temperature calculated from the heat flux was ~1580 C at B-64; the instrument at the second barrier position did not measure any temperature increase.

The mean delay time at the barrier start position was 175 ms.. The concentrated barrier configuration was effectively activated. Only three piles of stone dust were observed in the crosscut in the middle of the barrier. The stone dust was well distributed with heavy stone dust loadings observed on the mine floor throughout the barrier zone (see Appendix 24) and for a distance of ~10 m beyond the end position of the barrier (Figure 8.3.1c).

Figure 8.3.1c: Photograph in B-drift after LLEM #393

8.3.2 Concentrated barrier test: LLEM test #394

Test #394 with the concentrated barrier configuration installed in B-drift was similar to test #392 that used the distributed barrier configuration in B-drift; i.e., 21,3 m long 9,5% methane ignition zone with a 68% TIC coal/stone dust loading in B-drift and an 82% TIC coal/stone dust loading in A- and C-drifts. The static pressure test results for the various drifts are shown in Table 8.3.2a.

Table 8.3.2a

Peak static pressures for LLEM test #394

A drift		B drift		C drift	
Instr. Pos.	**Pressure (kPa)**	**Instr. Pos.**	**Pressure (kPa)**	**Instr. Pos.**	**Pressure (kPa)**
A1	173	B1	217	C1	173
A2	161	B2	145	C2	88
A3	108	B3	139	C3	114

A drift		B drift		C drift	
Instr. Pos.	**Pressure (kPa)**	**Instr. Pos.**	**Pressure (kPa)**	**Instr. Pos.**	**Pressure (kPa)**
A4	102	B4	86	C4	75
A5	70	B5	81	C5	64
A6	69	B6	63	C6	62
A7	64	B7	51	C7	51
A8	55	B8	45	C8	46
A9	55	B9	46	C9	46
A10	49	B10	43	C10	48

The average static pressure in B-drift was ~90 kPa. The decay in the static pressure for the various drifts is shown in Figure 8.3.2a.

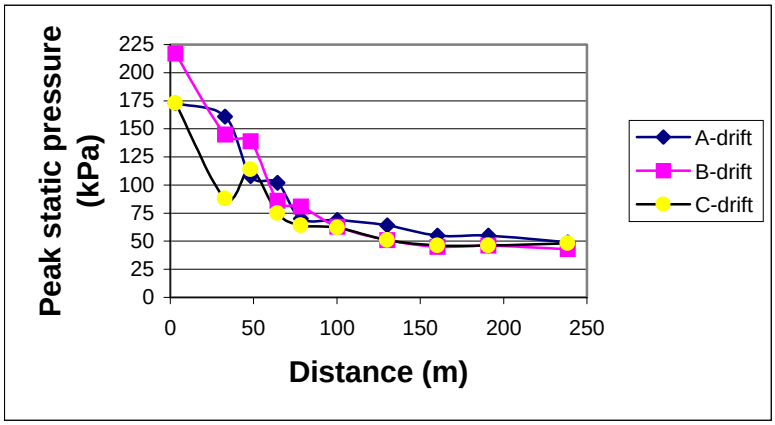

Figure 8.3.2a: Static pressure decay for LLEM test #394

Table 8.3.2b

Peak dynamic pressures for LLEM test #394

Instr. Distance (m)	Instr. Type	Dynamic Pressure (kPa)	Av. Dynamic Pressure (kPa)
A-49	BDP-1	57	57
C-34	BDP-6	30	30
B-41	Kistler	119	117
B-41	BDP-5	115	
B-73	Kistler	37	42
	BDP-2	47	
B-101	BDP-4	10	10
B-130	BDP-5	4	4

The peak dynamic pressure for LLEM test #394 is shown In Table 8.3.2b**.** The dynamic pressure in B-drift reduced from 115 kPa to 4 kPa over a 90 m distance which spanned three intersections.

The flame extended to ~110 m in B-drift, with flame into the first four cross-cuts toward A-drift and into the first three cross-cuts toward C-drift. Details of the flame sensor data are in Appendix 25. Flame propagation was stopped within the barrier and the flame extended no more than 30 m from the barrier start position. The total flame reduction was approximately 140 m in B-drift.

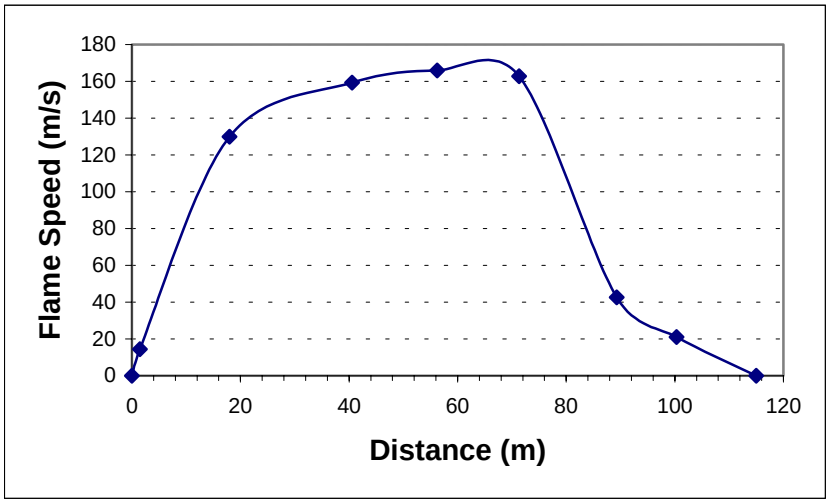

Figure 8.3.2b: Flame speed in B drift for LLEM test #394

The flame speed in B-drift is shown in Figure 8.3.2b. The flame reached a maximum flame speed of 166 m/s at 56 m. At the position of the first sub barrier, the flame speed was calculated as 140 m/s. The flame speed decreased rapidly within the barrier zone and was quenched near the outbye end of the barrier zone.

The calculated temperature was ~1560 C at B-64; the instrument at the second barrier position did not measure any temperature increase.

The mean delay time at the barrier start position was 147 ms. The concentrated barrier was effectively activated during this test. The stone dust was well distributed with heavy stone dust loadings observed on the mine floor throughout the barrier zone and beyond.

9 Conclusions

The major findings of the B-drift methane test results against the individually suspended barrier bags with the seal in crosscut 1 between B- and C-drifts are:

- The bags operated at dynamic pressures as low as 4 kPa..
- The static pressures in A-, B-, and C-drifts quickly balance to equal pressures except near the ignition position in B-drift.

- Bags suspended in the crosscuts did not distribute stone dust effectively in the areas where pressure equalization occurred.
- The bags in the drifts (A, B, and C) operated effectively
- The stone dust bag at position 29, just outbye of the methane ignition zone, operated and dispersed effectively, indicating a rapid time response prior to flame arrival.

A major conclusion from phase I of the program (methane explosion creating a single pressure source) is that the individual barrier bags will operate effectively when suspended close to the mine roof in a low seam (~2 m) multiple entry mine configuration. The effective distribution of the stone dust contained within the barrier bag is dependent on the distance of the barrier bag from the explosion source as well as the placement; i.e., whether the bag is suspended in a drift or in the crosscut.

Duplicate tests were also conducted during phase I to determine the effect of the individual barrier bag operations during the methane ignitions with and without the seal in place in crosscut 1 between B- and C-drifts. With the seal removed, an overall reduction in the dispersal efficiency of the bags resulted when initiating the methane ignitions from C-drift. For the B-drift ignitions, similar results were obtained; this was especially evident in A-drift where the removal of the seal in crosscut 1 reduced the reflective explosion wave and resulted in a reduction in the dispersal efficiency in total.

Phase II of the program to evaluate the bagged stone dust barrier systems against coal dust explosions was successfully completed at LLL. Two passive barrier design configurations were evaluated; the distributed barrier configuration and the concentrated barrier configuration. Each configuration was performance evaluated against an explosion using a 21,3 m long 9,5% methane ignition zone with a 119 m long 68% TIC coal/stone dust zone only loaded in B-drift and a second similar test with an additional 119 m long, 82% TIC dust zone in both A- and C-drifts. Both the distributed and concentrated barrier configurations were successful in stopping the coal dust explosion flame propagation within the barrier zones. In the triple-entry dust zone tests, the flame extended somewhat further than in the tests with only the B-drift dust loading.

The bagged stone dust barrier has thus proven successful in stopping flame propagation in small (5 m^2 gallery at Kloppersbos), medium (12 m^2 gallery at LLL), and large (20 m^2 gallery at Tremonia) explosion galleries. The results from the barrier evaluation programs that were

conducted at these facilities appear to have successfully resolved the potential concern regarding the adequacy of the barrier design and operation as a function of entry size and configuration (single entry or bord and pillar entries). Barrier operation is still dependent on the type and strength of the explosion to be extinguished. Furthermore, all barrier designs, including the stone dust barrier bag systems, have limits to their operational extremities.

10 References

Du Plessis, J.J.L. and Vassard, P.S. Assessment of the Dispersed Stone Dust Barrier. *SIMRAC Final Project Report COL 322.* Pretoria: CSIR Miningtek Kloppersbos

Gardon, R. *An Instrument for the Direct Measurement of Intense Thermal Radiation*. Review of Scientific Instruments, v. 24, pp. 366-370, 1953.

Greninger, N.B., Cortese, R.A. & Weiss, E.S. Suppression of dust explosions using triggered barriers in wide rectangular entries. *Proceedings of the 26th International Conference of Safety in Mines Research Institutes.* Katowice, 4 – 8 September 1995.

Margenburg, B. & du Plessis, J.J.L. Explosion tests with distributed stone dust bags (RSA) in the Explosion Gallery (20 m^2) Tremonia Experimental Mine, Dortmund. *Final Report.* 1996

Mattes, R.H., Bacho, A. & Wade, L.V. Lake Lynn Laboratory: construction, physical description and capability. USBM IC 8911, 1983 PPS 28.

Michelis, J., Margenburg, B. & du Plessis, J.J.L. Explosion tests with stone dust bags (RSA) in the Explosion Gallery (20 m^2) Tremonia Experimental Mine, Dortmund, Germany. *Continuation report.* January 1996.

Weiss, E. S., Cashdollar, K. L., Mutton, V. S., Kohli, D. R., and Slivensky, W.A. Evaluation of Reinforced cementitious seals. NIOSH RI 9647. August 1999.